Defense Nuclear Agency
Alexandria, VA 22310-3398

DNA-TR-89-289

Shock Induced Cavitation

Vincent J. Cushing
Cushing Associates, Inc.
153 Williams Drive
Annapolis, MD 21401

February 1991

Technical Report

CONTRACT No. DNA 001-80-C-0070

Destroy this report when it is no longer needed. Do not return to sender.

PLEASE NOTIFY THE DEFENSE NUCLEAR AGENCY, ATTN: CSTI, 6801 TELEGRAPH ROAD, ALEXANDRIA, VA 22310-3398, IF YOUR ADDRESS IS INCORRECT, IF YOU WISH IT DELETED FROM THE DISTRIBUTION LIST, OR IF THE ADDRESSEE IS NO Llonger EMPLOYED BY YOUR ORGANIZATION.

REPORT DOCUMENTATION PAGE

Form Approved
OMB No. 0704-0188

1. AGENCY USE ONLY *(Leave blank)*	2. REPORT DATE	3. REPORT TYPE AND DATES COVERED
	910201	Technical 790106 - 831231

4. TITLE AND SUBTITLE

Shock Induced Cavitation

5. FUNDING NUMBERS

C-DNA 001-80-C-0070
PE-62715H
PR-H02CAXS
TA-X
WU-DH004592

6. AUTHOR(S)

Vincent J. Cushing

7. PERFORMING ORGANIZATION NAME(S) AND ADDRESS(ES)

Cushing Associates, Inc.
153 Williams Drive
Annapolis, MD 21401

8. PERFORMING ORGANIZATION REPORT NUMBER

CA 101FR

9. SPONSORING/MONITORING AGENCY NAME(S) AND ADDRESS(ES)

Defense Nuclear Agency
6801 Telegraph Road
Alexandria, VA 22310-3398
SPWE/Tremba

10. SPONSORING/MONITORING AGENCY REPORT NUMBER

DNA-TR-89-289

11. SUPPLEMENTARY NOTES

This work was sponsored by the Defense Nuclear Agency under RDT&E RMSS Code B344080462 H02CAXSX 38801 H25904.

12a. DISTRIBUTION/AVAILABILITY STATEMENT

Approved for public release; distribution is unlimited.

12b. DISTRIBUTION CODE

13. ABSTRACT *(Maximum 200 words)*

Shock test planning for surface ships renewed interest in shock induced cavitation as a mechanism of damage to naval ships. To assist DNA in formulating and conducting a program for further investigation of cavitation, there is provided here: a review of past theory and experimental data, extending back to WWII; a refinement of theory providing for after flow in the incident shockwave; a review of hull plate loading involving local cavitation; and predictions of secondary pressures and impulses generated by combined effects of bulk cavitation and sea-bottom reflection. Sea-bottom reflection characteristics for a specific shock test site are generally known poorly. Analysis indicates that an unfortunate choice of test site could produce large reflection-and-cavitation effects.

14. SUBJECT TERMS

Bulk Cavitation
Hull Plate Loading
Spallation
Local Cavitation
Shock Induced Cavitation

15. NUMBER OF PAGES

66

16. PRICE CODE

17. SECURITY CLASSIFICATION OF REPORT	18. SECURITY CLASSIFICATION OF THIS PAGE	19. SECURITY CLASSIFICATION OF ABSTRACT	20. LIMITATION OF ABSTRACT
UNCLASSIFIED	UNCLASSIFIED	UNCLASSIFIED	SAR

CLASSIFIED BY:

N/A since Unclassified

DECLASSIFY ON:

N/A since Unclassified

DISTRIBUTION LIST UPDATE

This mailer is provided to enable DNA to maintain current distribution lists for reports. We would appreciate your providing the requested information.

☐ Add the individual listed to your distribution list.

☐ Delete the cited organization/individual.

☐ Change of address.

NOTE:
Please return the mailing label from the document so that any additions, changes, corrections or deletions can be made more easily.

NAME: _____

ORGANIZATION: _____

OLD ADDRESS	**CURRENT ADDRESS**
_____	_____
_____	_____
_____	_____

TELEPHONE NUMBER: ( ) _____

SUBJECT AREA(s) OF INTEREST:

_____	_____
_____	_____
_____	_____

DNA OR OTHER GOVERNMENT CONTRACT NUMBER: _____

CERTIFICATION OF NEED-TO-KNOW BY GOVERNMENT SPONSOR (if other than DNA):

SPONSORING ORGANIZATION: _____

CONTRACTING OFFICER OR REPRESENTATIVE: _____

SIGNATURE: _____

CUT HERE AND RETURN

PREFACE

Shock test planning for the Navy surface ships prompted new interest in the phenomena of Underwater Cavitation as a damage augmenting process. Results have been transmitted via letter reports during the planning process. This is the formal Final Report.

The following tasks were carried out:

1. Review past theory and experimental data;
2. Extend Bulk Cavitation theory for secondary pressures owing to momentum accretion and afterflow on bulk cavitation region's closure front;
3. Extend theory to include hull surface's inertia and compliance;
4. Assist in design of bulk cavitation experiments; and monitor DNA's other cavitation efforts.

Predictions are made for possible effects of Bulk Cavitation in a typical shock test.

Technical monitors have been Lt. Robert Elsbernd, USN and Lt. Dennis Sobota, USN.

The Underwater Explosives Research Division of David Taylor Research & Development Center has considerable background information on Bulk Cavitation and Hull Plate Loading. The writer is grateful for recent help provided by that Division's John Wise, Robert Walker and John Gordon, and also for early help by W. W. Murray and Heinrich Schauer.

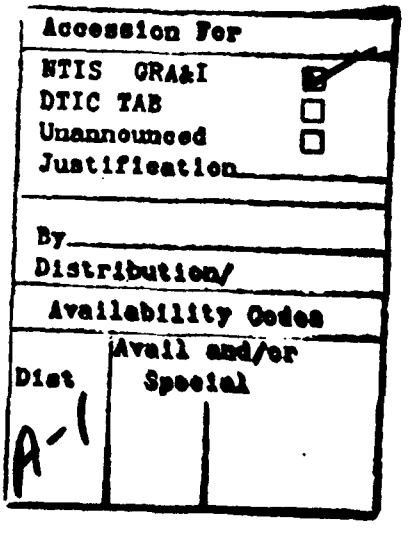

CONVERSION TABLE

Conversion factors for U.S. Customary to metric (SI) units of measurement.

MULTIPLY ⟶ BY ⟶ TO GET
TO GET ⟵ BY ⟵ DIVIDE

angstrom	1.000 000 X E -10	meters (m)
atmosphere (normal)	1.013 25 X E +2	kilo pascal (kPa)
bar	1.000 000 X E +2	kilo pascal (kPa)
barn	1.000 000 X E -28	meter^2 (m^2)
British thermal unit (thermochemical)	1.054 350 X E +3	joule (J)
calorie (thermochemical)	4.184 000	joule (J)
cal (thermochemical)/cm^2	4.184 000 X E -2	mega joule/m^2 (MJ/m^2)
curie	3.700 000 X E +1	giga becquerel (GBq)*
degree (angle)	1.745 329 X E -2	radian (rad)
degree Fahrenheit	$t_k=(t°f+459.67)/1.8$	degree kelvin (K)
electron volt	1.602 19 X E -19	joule (J)
erg	1.000 000 X E -7	joule (J)
erg/second	1.000 000 X E -7	watt (W)
foot	3.048 000 X E -1	meter (m)
foot-pound-force	1.355 818	joule (J)
gallon (U.S. liquid)	3.785 412 X E -3	meter^3 (m^3)
inch	2.540 000 X E -2	meter (m)
jerk	1.000 000 X E +9	joule (J)
joule/kilogram (J/kg) (radiation dose absorbed)	1.000 000	Gray (Gy)**
kilotons	4.183	terajoules
kip (1000 lbf)	4.448 222 X E +3	newton (N)
kip/inch^2 (ksi)	6.894 757 X E +3	kilo pascal (kPa)
ktap	1.000 000 X E +2	newton-second/m^2 ($N-s/m^2$)
micron	1.000 000 X E -6	meter (m)
mil	2.540 000 X E -5	meter (m)
mile (international)	1.609 344 X E +3	meter (m)
ounce	2.834 952 X E -2	kilogram (kg)
pound-force (lbf avoirdupois)	4.448 222	newton (N)
pound-force inch	1.129 848 X E -1	newton-meter (N·m)
pound-force/inch	1.751 268 X E +2	newton/meter (N/m)
pound-force/foot^2	4.788 026 X E -2	kilo pascal (kPa)
pound-force/inch^2 (psi)	6.894 757	kilo pascal (kPa)
pound-mass (lbm avoirdupois)	4.535 924 X E -1	kilogram (kg)
pound-mass-foot^2 (moment of inertia)	4.214 011 X E -2	kilogram-meter^2 ($kg·m^2$)
pound-mass/foot^3	1.601 846 X E +1	kilogram/meter^3 (kg/m^3)
rad (radiation dose absorbed)	1.000 000 X E -2	Gray (Gy)**
roentgen	2.579 760 X E -4	coulomb/kilogram (C/kg)
shake	1.000 000 X E -8	second (s)
slug	1.459 390 X E +1	kilogram (kg)
torr (mm Hg, 0°C)	1.333 22 X E -1	kilo pascal (kPa)

* The becquerel (Bq) is the SI unit of radioactivity; 1 Bq = 1 event/s.
**The Gray (Gy) is the SI unit of absorbed radiation.

TABLE OF CONTENTS

LIST OF ILLUSTRATIONS

SHOCK INDUCED CAVITATION

SECTION 1

INTRODUCTION

During shock test planning for the Navy surface ships, there was renewed interest in the phenomenon of bulk cavitation as a damage augmenting process. Results of the subject contract were transmitted via letter reports during the planning process. This is the formal Final Report.

The following tasks were carried out:

1. Review past theory and experimental data;
2. Extend Bulk Cavitation theory for secondary pressures owing to momentum accretion and afterflow on bulk cavitation region's closure front;
3. Extend theory to include hull surface's inertia and compliance;
4. Assist in design of bulk cavitation experiments; and monitor DNA's other cavitation efforts.

Predictions are made for possible effects of Bulk Cavitation in a typical shock test.

Bulk Cavitation theory is provided in Section 2. The Closure process, with consequent water hammer, is described in Section 3.

The REFERENCES cite the history of Bulk Cavitation, Local Cavitation and hull plate loading. Past cavitation experiments are discussed in Section 4. Laboratory experiments, using an exploding wire to simulate a nuclear-like steam bubble, are also discussed.

Work to date by all has involved the effects of the direct shock wave only — unfettered by secondary shock waves owing to bottom reflection. Bottom reflections, see Section 5, can play a substantial role. Further investigation is required.

Fundamentals of hull plate loading associated with local cavitation are discussed in Section 6. Quantitative detail involves diffraction analysis, not yet achievable in closed form analysis. Simplified, closed form analyses are discussed. Computer codes (including diffraction phenomena) and results are discussed.

The Appendix lists a Z100 Basic code formulated to determine, for a spherical explosion, the extent of Bulk Cavitation as well as the depth of final closure and intensity of water hammer shocks generated.

SECTION 2

BULK CAVITATION

The phenomena of Bulk Cavitation and Closure have been described in work dating back to 1943[15,26,27,45]. For a brief description of the phenomena we follow reference 15.

Consider a compressive underwater shockwave moving toward a free water surface as shown in figure 1a. We consider a shock wave with initial pressure p_o followed by an exponential decay of duration t_w. At distances from the explosive source which are of practical interest, the velocity of the shockwave is essentially the speed of sound, c, in water. Hence, the wavelength λ of the incident shockwave is

$$\lambda = ct_w \quad . \tag{1}$$

2.1 UPPER CAVITATION DEPTH.

Just before shock front arrival at the surface, the total absolute pressure is as depicted in figure 1b. When the compressive front arrives at the surface, boundary conditions require that a rarefactive wave be reflected. Just after reflection from the surface, the total pressure is as depicted in figure 2. We note that as the rarefactive front, of strength $-p_o$, moves down into the water: (1) the pressure beneath the rarefaction front is that owing to the waning portions of the incoming wave; (2) above the rarefaction front, the total pressure remains p_a (atmospheric pressure) at the surface and progressively falls as the rarefaction front is approached. Below some point, shown as Z_o, the total absolute pressure is negative — the water goes into tension.

Since seawater cannot withstand appreciable tension, the water ruptures; the pressure in the ruptured water falls to vapor pressure — zero for all practical purposes.

All types of incident shock waves do not necessarily result in cavitation. If the peak pressure is sufficiently large and the decay wavelength λ is exceedingly long, hydrostatic pressure will rise faster than the incident wave decays, and total pressure will monotonically increase with depth — as indicated by figure 3's curve III. A shorter wavelength may result in pressure lowering as shown in curve II, but zero pressure is never reached. Most practicable explosions, including nuclear, have pressure/wavelength combinations (by the time the free water surface is encountered) such that zero pressure is achieved and bulk cavitation commences at some depth Z_o.

Figure 4 depicts an incident shockwave rising vertically to the free water surface Z_s, which is initially at zero depth. If the incident shock has a particle velocity of u_o, upon reflection the surface Z_s initially moves upward with velocity $2u_o$. When the reflected wave reaches the onset depth Z_o, the water ruptures; total pressure at the depth is substantially zero — the vapor pressure of water at ambient temperature.

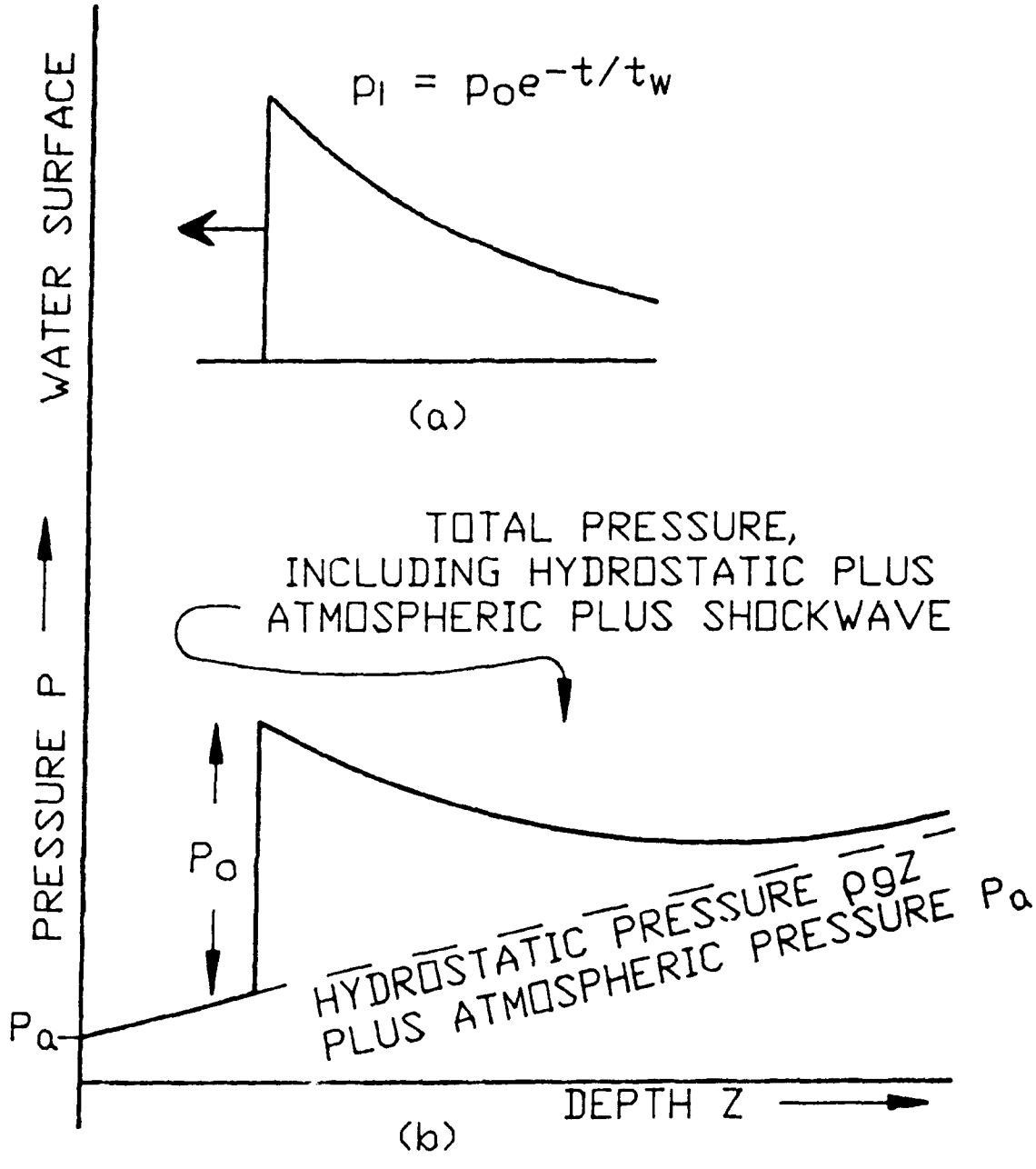

Figure 1. (a) Compressive underwater shockwave moving toward a free surface. Peak pressure p_o; decay time constant t_w. (b) Total absolute pressure just before shock arrival at free surface.

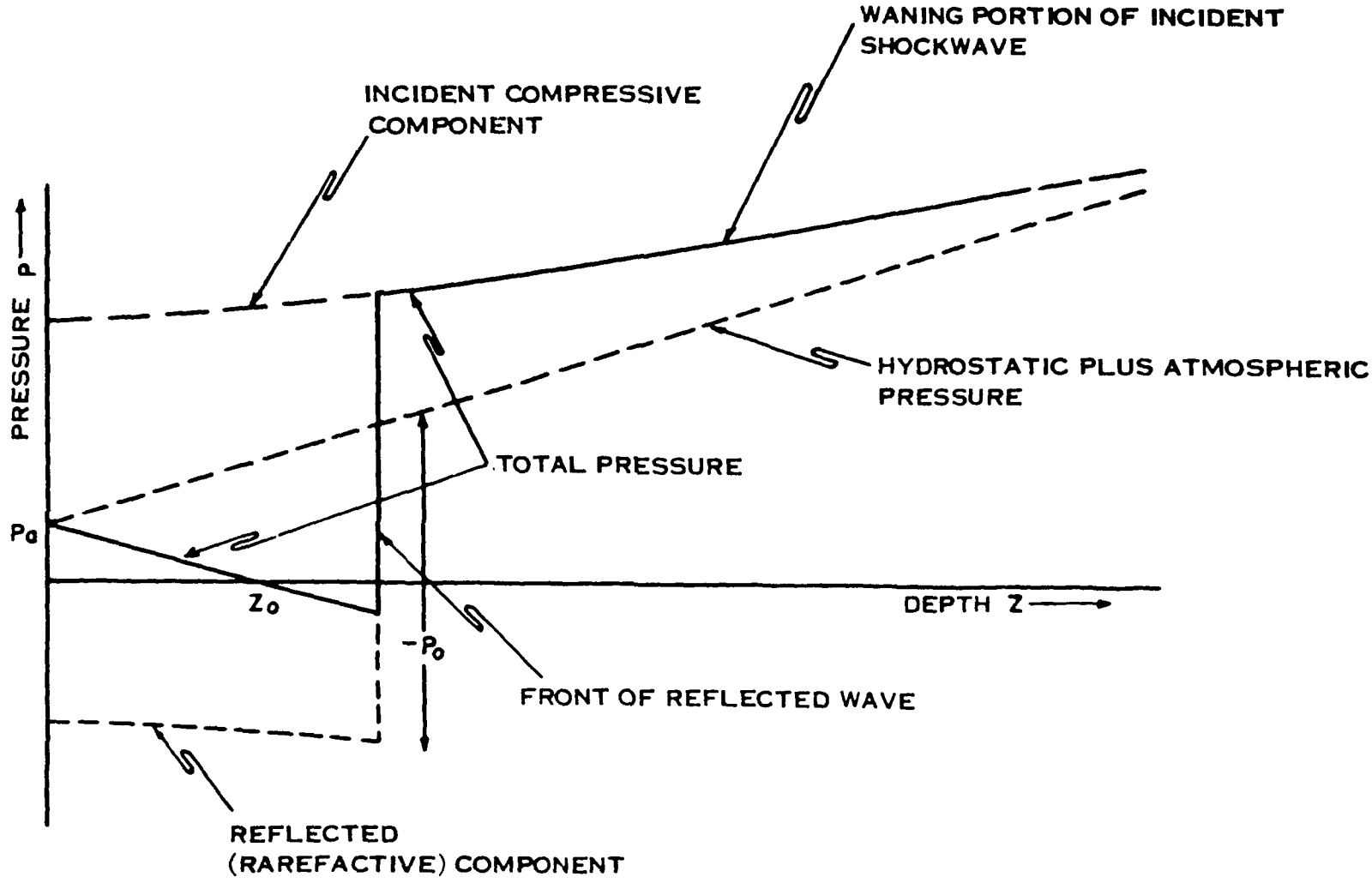

Figure 2. Total pressure p — the superposition of pressures: atmospheric, hydrostatic, incident shockwave, reflected shockwave — as a function of depth z after the incident shockwave has reflected from the free water surface. *Here, atmospheric and hydrostatic pressures are shown as absolute;* shockwave pressures are shown as gauge, i.e., relative to the sum of atmospheric and hydrostatic pressures.

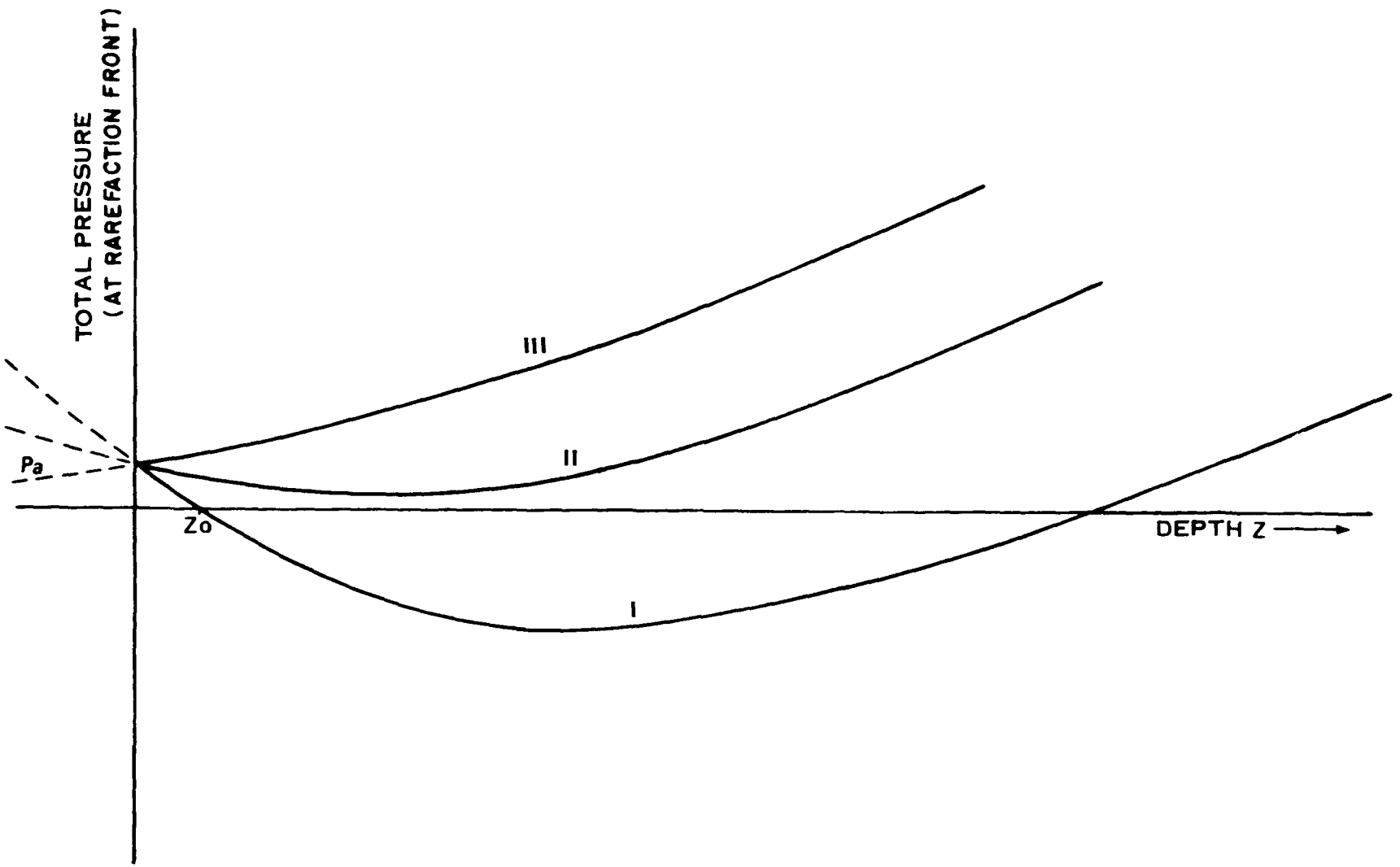

Figure 3. Total pressure at reflected rarefaction front as a function of depth z.

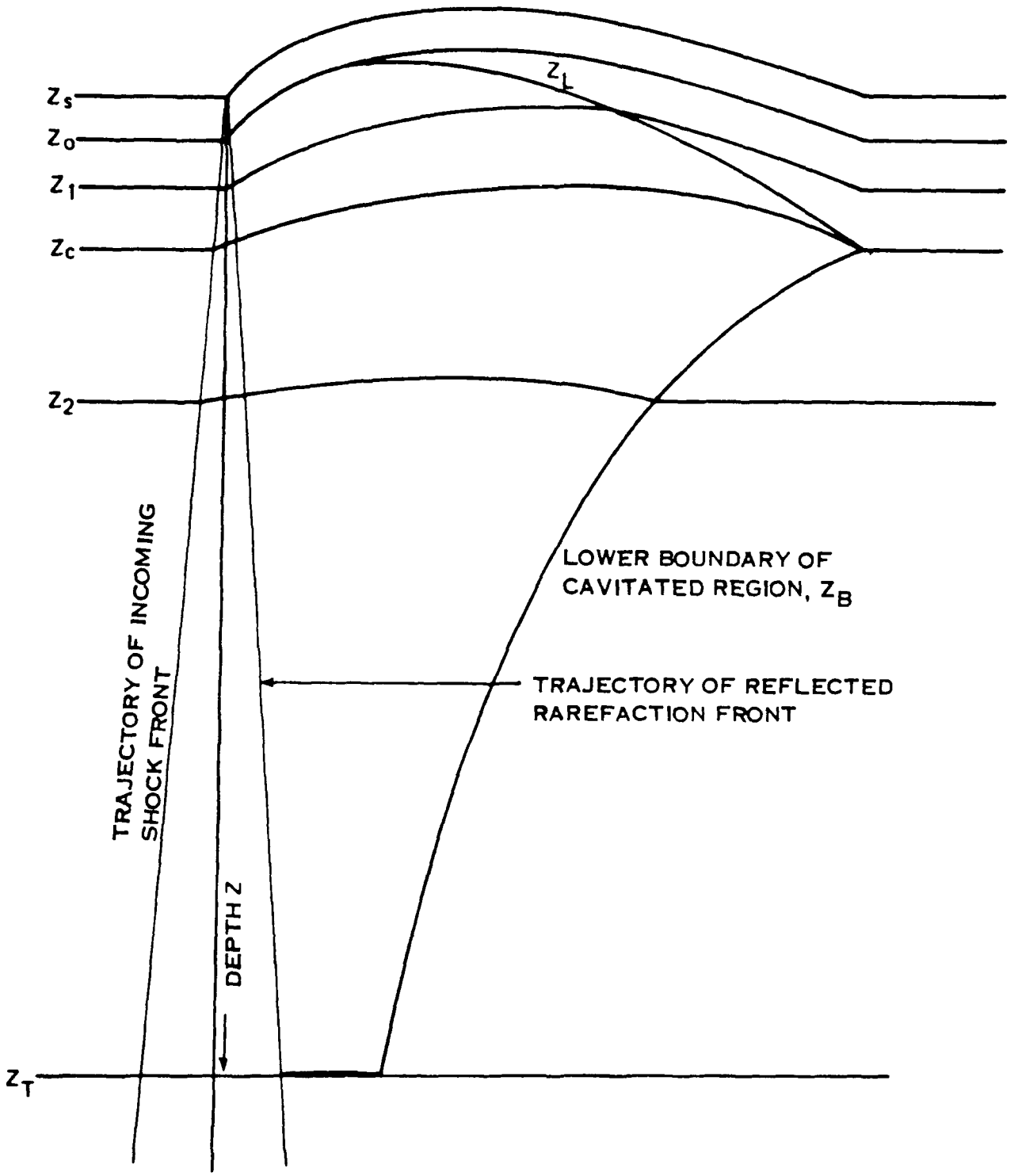

Figure 4. Motion of water particles at various depths, ranging from z_s (the water surface) to z_o (the depth of cavitation onset), z_c (depth of ultimate cavitation closure) and z_T (terminal depth beyond which there is no cavitation). The particle originally at depth z_1 is typical of the water particle which is accreted to the lower boundary z_L of the spall. The water particle of depth z_2 follows a ballistic trajectory till it falls back to its original depth.

2.2 ACCRETION TO SPALL.

At that instant there is a liquid layer of water — a spall of thickness (Z_s-Z_o) — moving upward with almost the velocity $2u_o$. The decelerating forces are two: (1) boundary forces — atmospheric pressure at the upper surface and negligible vapor pressure at the lower surface; and (2) body forces — gravitational force acting throughout the liquid layer.

As shown in figure 4, the spall's lower surface is denoted by Z_L. (Z_s-Z_L) — the spall's thickness — is initially equal to (Z_s-Z_o). We shall see that this thickness grows. As it does the added deceleration owing to atmospheric pressure at the upper surface becomes relatively less compared with the body force of gravity. Hence the spall deceleration will asymptotically approach 1g.

The particle velocity u at any point of the incoming shockwave is, since the acoustic approximation is adequate

$$u = p/\rho c \quad , \tag{2}$$

where ρ is the water density, and c is the speed of sound. As the reflected rarefaction front moves into water deeper than that at Z_o, it encounters the waning portions of the incoming wave — where the particle velocity has fallen to u, with u described by equation 2. Accordingly, the rarefaction front leaves behind it cavitated water whose initial upward velocity, or launch velocity, is 2u. Hence the launch velocity continuously falls as the rarefaction penetrates the waning portions of the incoming wave.

Since the cavitated region is entirely at vapor pressure, the deceleration of the launched, cavitated water is not affected by pressure forces, only gravitational forces. Hence each cavitated water particle follows a ballistic trajectory — with exactly one g of deceleration.

We recall that the liquid spall decelerates asymptotically toward 1g — at all times it decelerates faster than 1g. Hence the liquid spall is continuously decelerating into underlying cavitated water. The spall thickness grows owing to accretion of the underlying cavitated water. Figure 4 depicts that the spall's lower surface Z_L is continuously colliding with underlying spalled water. Spall growth continues in this fashion until it accretes the cavitated particle which had been launched from depth Z_c, from what we shall see is the cavitation closure depth.

2.3 LOWER CAVITATION DEPTH.

The reflected rarefaction front, as shown in figure 4, continually produces cavitation until some lower depth Z_T, the cavitation termination depth. Beyond that depth the hydrostatic pressure is too large to allow the total absolute pressure to reach zero. The water below Z_T remains liquid at all times.

The cavitated water just above Z_T has a very small launch velocity and a very brief ballistic trajectory. It soon falls back on the underlying liquid water. Analogous to

behavior of the accreting spall, the underlying liquid surface moves upward owing to cumulative accretion of water that had been in ballistic trajectory in the cavitated region.

2.4 WATER HAMMER,

The lower cavitation boundary rises while the spall's lower surface Z_L falls — until eventually there is no cavitated region left. The particle velocity on the lower cavitation boundary is, to a first approximation, zero. The particle velocity on the upper cavitation boundary is effectively the velocity of the decelerating spall. Hence at time t_c there is a water hammer as the spall impacts the quiescent lower boundary. (Actually the particle velocity of the lower boundary is not exactly zero. The computer program listed in the Appendix takes the actual velocity into account.)

Figure 5 is identical to figure 4 — except that the velocity of the incoming and reflected fronts is assumed to be infinite; i,e., the duration of the cavitation-producing process is assumed negligible compared with spall flight duration and the cavitation closure and water hammer processes. This simplification has enabled a closed form solution [15,46] of the bulk cavitation process. Results compare well with experiment [43,47].

As shown in figure 4, time t is measured from the moment the incoming shockwave reaches the water surface. Depth Z is measured from the initial position of the free surface.

The figure shows the Z-t trajectories of the incoming shock front and also the reflected rarefaction front. These waves move at velocity c, the speed of sound in water -- about 1,500 m/sec. Cavitation conditions exist when the reflected wave reaches the onset depth Z_o. Below that depth the water vaporizes when the rarefaction front passes.

Ultimately the upper, spalled layer will hammer the underlying liquid water beneath the boundary Z_B; the dynamics of the process produce secondary underwater pressure waves owing to this progressive water hammer.

2.5 TRAPPED ENERGY.

Depending on explosive yield and depth of burst, a large fraction of the total incident shock wave energy can be stored temporarily as kinetic energy and/or gravitational potential energy (of the overlying spall and also of the cavitated particles) during the bulk cavitation process; and the stored energy is re-emitted later during the water hammer process when the cavitation closes.

Bulk Cavitation's late-time secondary waves have produced extensive damage to ships during tests at HARDTACK Umbrella and in subsequent HE tests. This prompted earlier investigations. The program for the ARKANSAS shock tests prompted DNA's renewed interest in Bulk Cavitation.

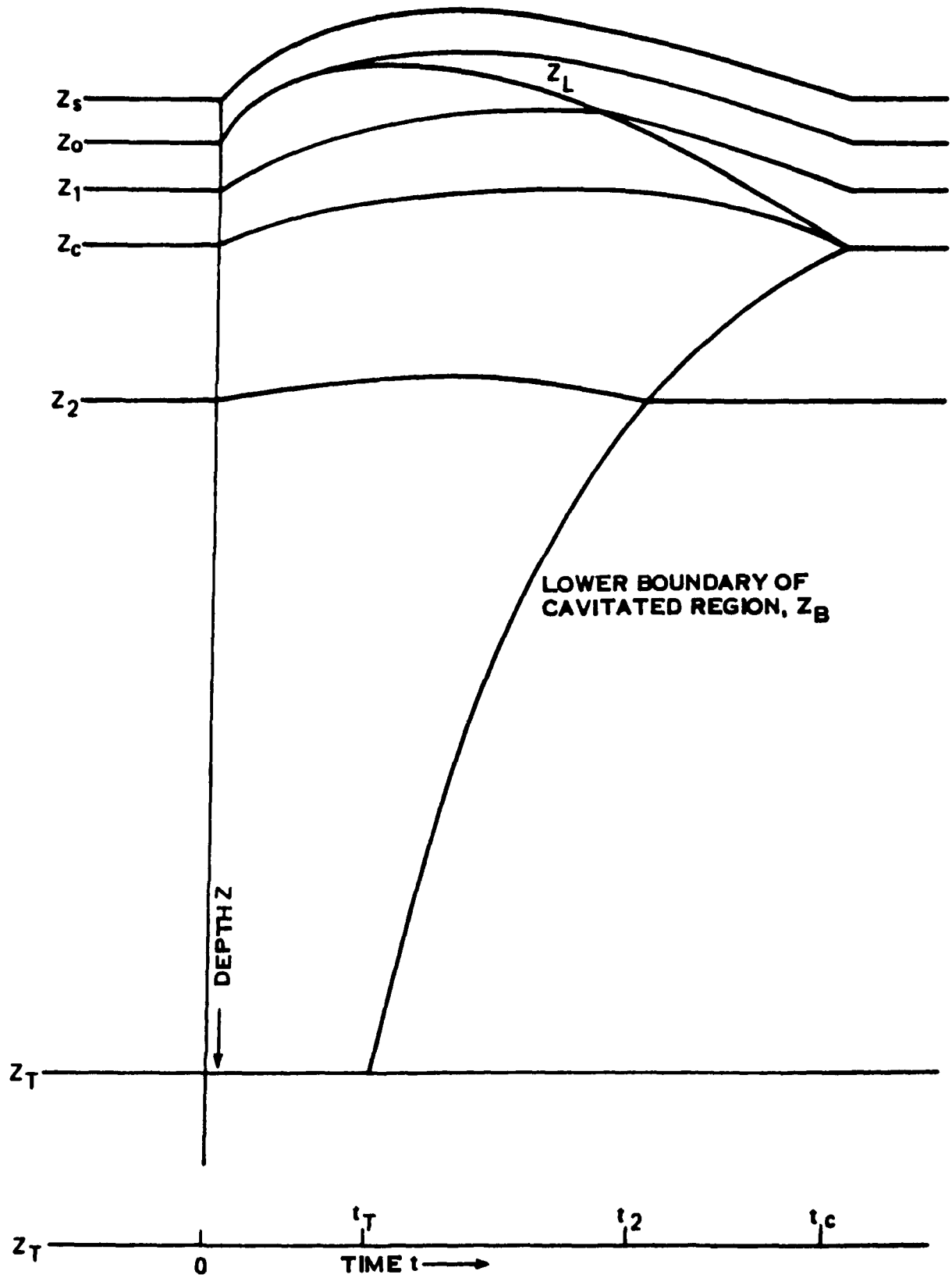

Figure 5. Water particle trajectories under the approximation that the transit time of the rupturing rarefaction front is negligible compared with the trajectory times of the cavitated water.

2.6 SPHERICAL EXPLOSIONS.

Figure 6 shows the more practical situation of a spherical explosion. The incident shock first arrives at the surface directly above the explosive, at surface-zero (SZ). Launch velocity of the spall is maximum there: it takes maximum time for the spall to complete its trajectory before impacting with the underlying water.

As we increase horizontal distance from SZ, the incident shock arrives later, it is weaker and its angle of incidence with the surface results in a decreasing spall launch velocity. The consequence is in figure 7, which shows the time of closure T_c as a function of horizontal radius from surface-zero. Also shown is the time of arrival T_1 of the incident shockwave. We see that cavitation closure first occurs at radius X_{c1} at time T_{c1}.

Figure 8 shows the maximum surface excursion and the time of maximum excursion for this explosion configuration.

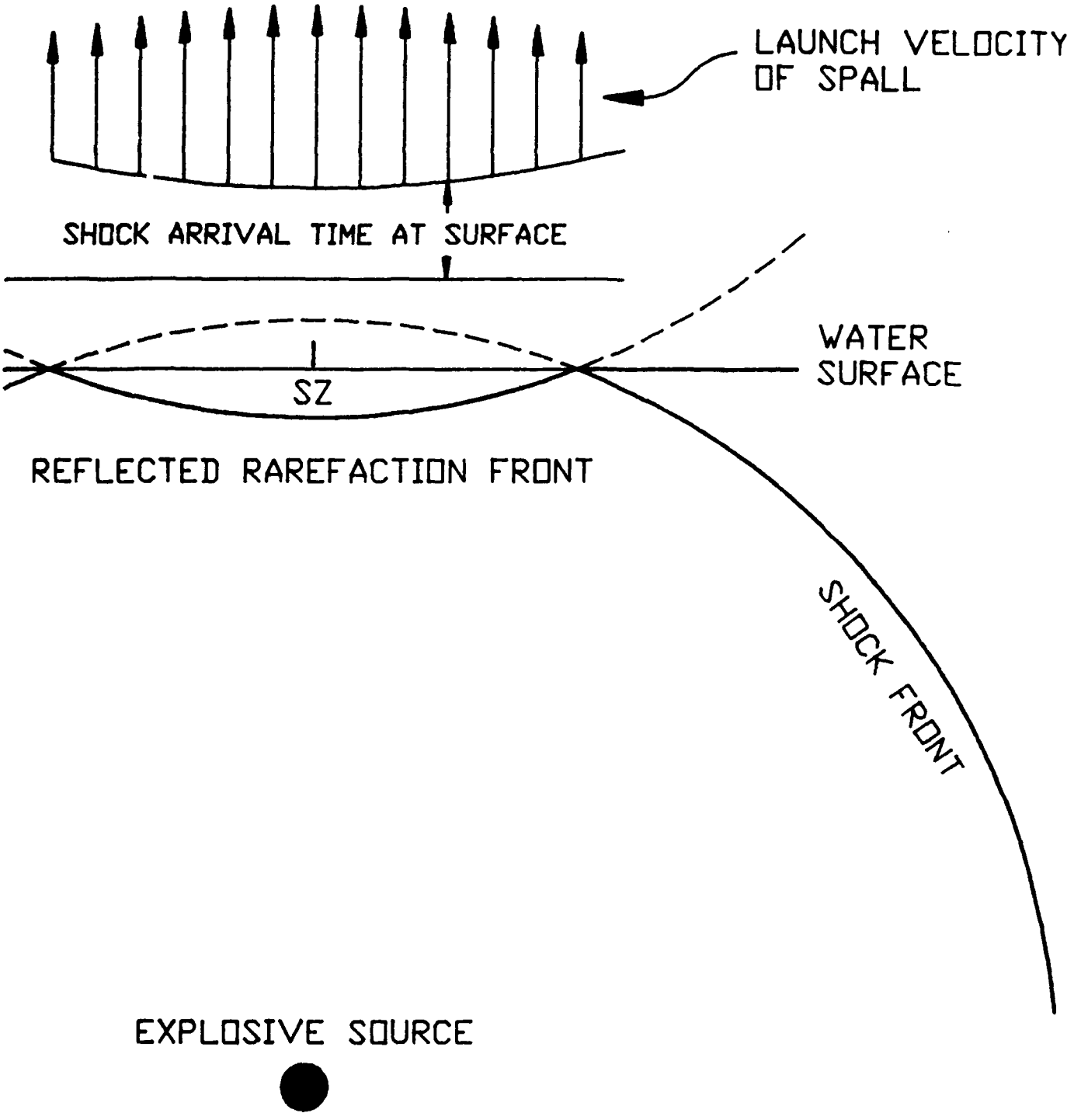

Figure 6. Geometry for analysis of spherical explosions.

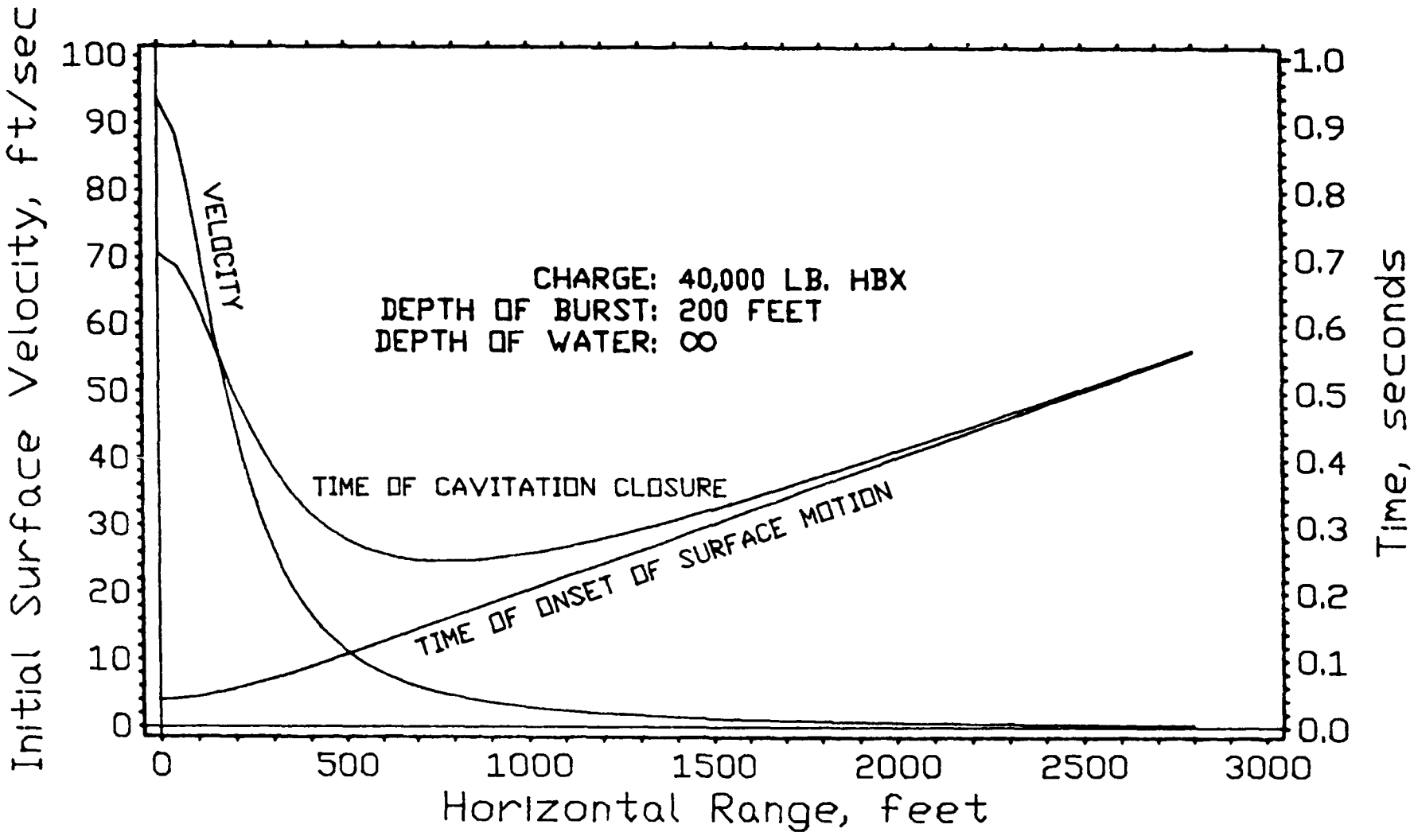

Figure 7. Some variables as a function of horizontal range for a spherical explosion.

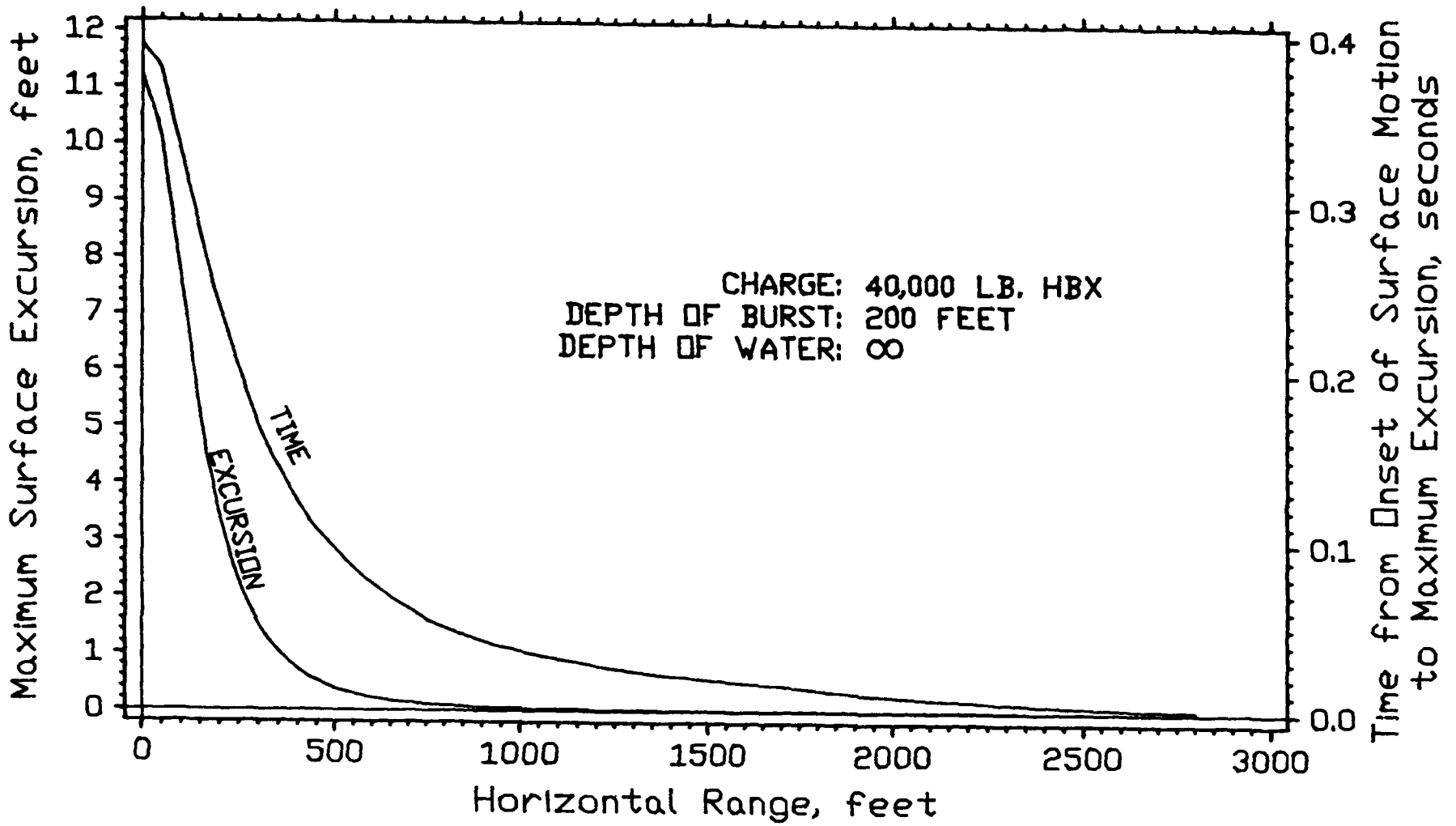

Figure 8. Some variables as a function of horizontal range for a spherical explosion.

SECTION 3

CAVITATION CLOSURE

3.1 PLANAR SHOCKWAVE.

An underwater shockwave, at distances from the explosive source which are of interest, behaves virtually as an acoustic wave. In practice the wave has a shock rise to peak pressure p_o, followed by an exponential-like decay. When such an acoustic wave is reflected from a rigid surface (1) the wave's momentum (total impulse) is reversed, and (2) the wave's kinetic energy is conserved. A corollary of this is that the wave's shape (magnitude and duration) is preserved.

When an underwater shock wave is reflected from a free surface, where negative pressure cannot exist in the medium, spallation or cavitation occurs. The wave's energy becomes stored in the gravitational energy of the spall, and the energy is returned (with considerable dissipation) during the closure process. The result is, eventually, a reflected wave which is compressive. The wave's (1) kinetic energy is not conserved, and (2) while the magnitude of momentum is conserved, the momentum is reversed. A corollary of this is that wave shape is not preserved.

For analysis we assume the Instant Cavitation depicted in Section 2's figure 5 (page 9); i.e., the travel time of the cavitating wave front — which moves at sound speed — is negligible compared with the duration of spallation and cavitation. The particle velocity u(Z) at depth Z in the cavitated region (for incident wave with shock rise to pressure p_o, and exponential decay with wavelength λ) is [15]

$$u(Z) = -(p_a + \rho gZ + 2p_o e^{-2Z/\lambda})/\rho c \quad , \tag{3}$$

where p_a is atmospheric pressure, ρgZ is hydrostatic pressure at depth Z and ρc is the water's acoustic impedance.

In the cavitated region the pressure is constant vapor pressure of water. There is no pressure gradient; hence, each cavitated water particle follows a ballistic trajectory. The particle's flight time (the time until gravity reverses the particle's momentum and it falls back to its original depth Z) is

$$t_f = 2u(Z)/g \quad . \tag{4}$$

For water at depths above the closure point, the water particle doesn't get a chance to complete its ballistic flight; the higher acceleration (owing to the added force of atmospheric pressure on top) of the overlying spall causes the particle to accrete to the spall's underside before flight time is completed. Particles launched at the closure depth complete the ballistic flight. Particles launched below the closure point also do not complete the ballistic flight; they accrete to the rising underlying water surface. The front of this accretion-by-fallback is the bulk cavitation lower closure front.

The water particle at closure depth Z_c is the last particle to complete its bal-

listic flight time. That particle accretes its mass and momentum at time

$$t_f(Z_c) = 2u(Z_c)/g \quad . \tag{5}$$

For short wavelength shock waves, the hydrostatic pressure and the atmospheric pressure are negligible compared with the 'pressure' component (see equation 2). Hence the flight time is

$$t_f(Z_c) = 4p_o/(\rho gc)e^{-2Z_c/\lambda} \quad . \tag{6}$$

3.2 SPHERICAL SHOCKWAVE.

In Section 2 it was pointed out that there is a radius (about surface zero) where cavitation closure and water hammer first occur. Figure 9 shows the spall and the underlying water in the neighborhood of this radius X_{c1} of first closure. Figure 9a depicts the situation just prior to first impact; 9b depicts it immediately after first impact. Closure progresses inward with instantaneous contact point X_i, and outward with contact point X_o.

Immediately after first impact, X_i and X_o travel approximately horizontally with infinite velocity and thereafter progressively slow down.

The outward travelling point X_o cannot move slower than the horizontal velocity of the incident shockwave, which travels at the speed of sound in water. Thus the outward travelling contact point monotonically slows to mach 1. However, as it approaches mach 1 the distance from the explosion center and the angle of incidence with the surface are such that the energy stored in the cavitation process is negligible, and the consequent water hammer at closure is negligible.

The inward travelling closure point X_i is not limited by the speed of sound in water. It may fall to and below mach 1. Distance and angle of incidence considerations permit appreciable stored energy and final water hammer. Indeed, the horizontal radius X_{m1} at which the contact point is travelling at mach 1 is particularly hazardous since the hammer pressure theoretically increases without bound at that radius[15].

In simple analyses it is assumed that the horizontal motion of cavitated water particles is negligible compared with the vertical motion. Figure 10 depicts the mach wave generated by the supersonically (in water) travelling closure point. Figure 10 shows the vertical velocities of the spall (u_s) and the underlying water (u_u). Figure 10's equation 4 shows the particle velocity normal to the mach front and to the reflected mach front. Equation 6 shows that the hammer pressure P_h increases without bound as the closure mach number M slows down and approaches unity. Even so, equations 9 and 10 show that the hammer impulse I_o below closure depth Z_c is bounded. Above closure depth the hammer impulse I is proportional to the depth Z below the water surface.

If a vessel's structure is pressure sensitive, it is at risk of self damage if it launches an underwater depth charge so as to place itself at the mach 1 distance. A

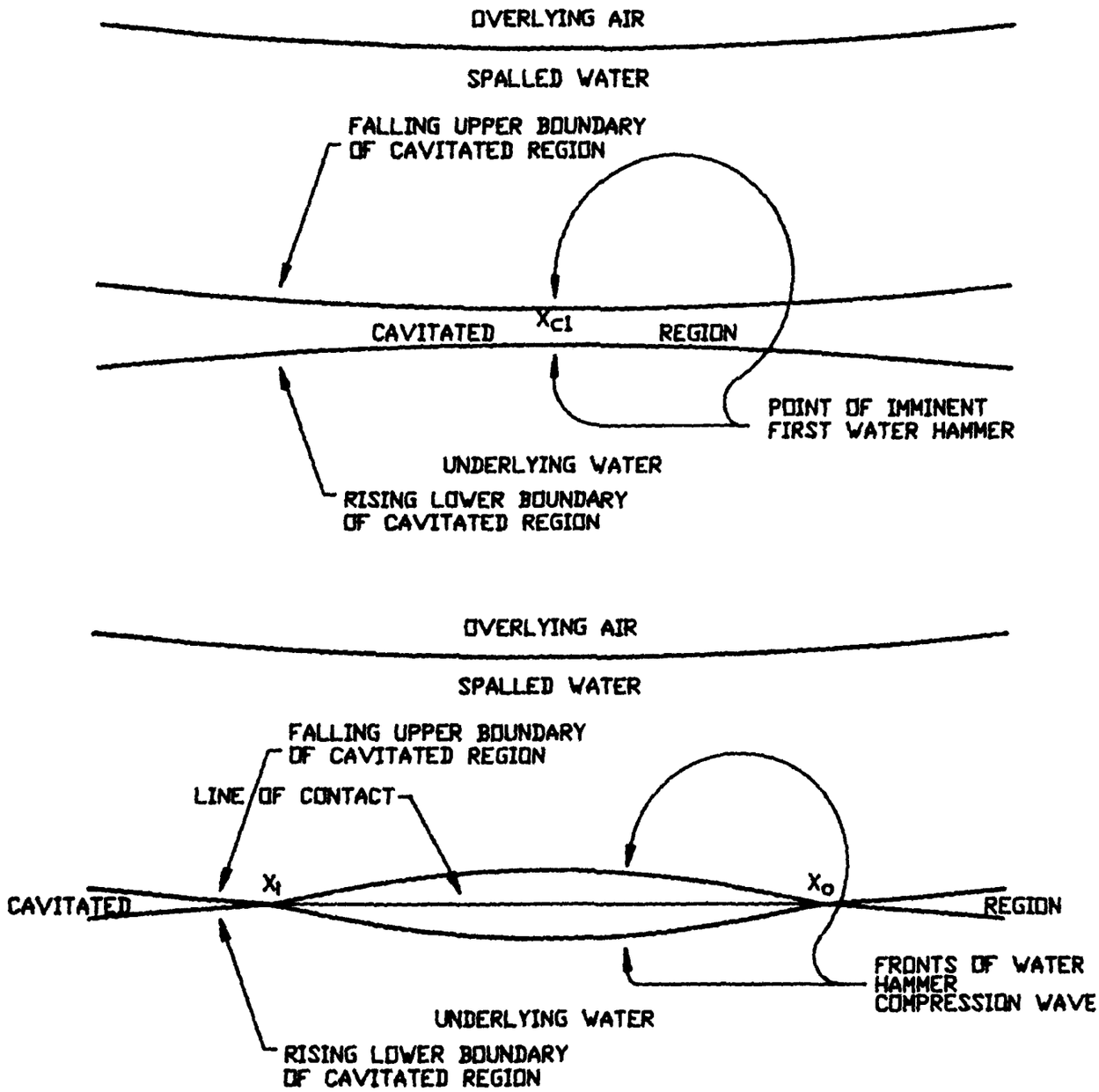

Figure 9. Spall and underlying water in the neighborhood of radius of first closure, X_{c1}, where water hammer first occurs.

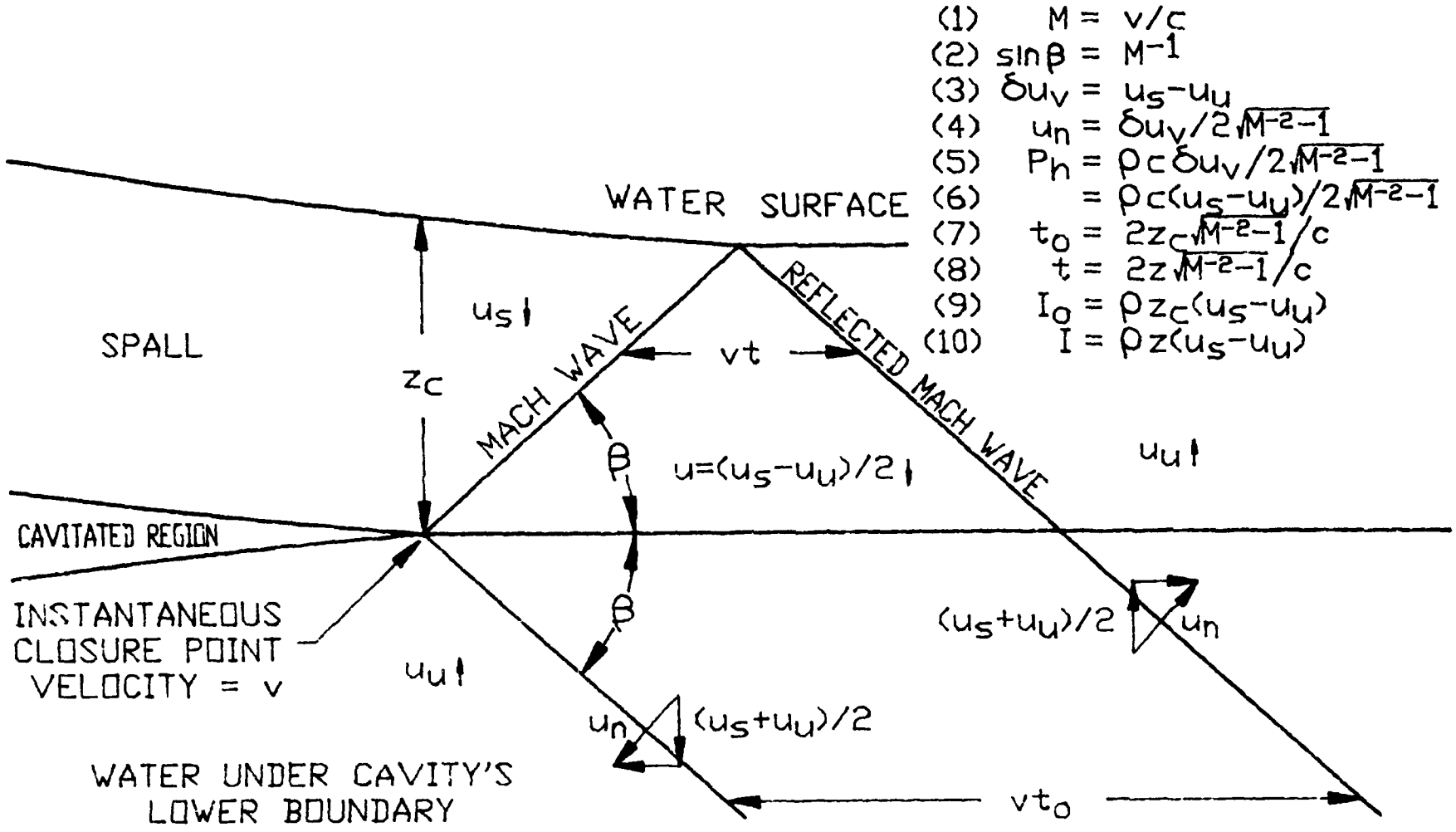

Figure 10. Mach wave generated by supersonically travelling locus of closure.

target vessel is most vulnerable if placed at that location. There is less hazard if the vessel's structure is impulse sensitive.

Figure 11 graphs the closure mach number and the time of closure for a 40,000 LB. HBX charge. The right ordinate is negative for the inward travelling mach front, and positive for the outward front.

Figure 12 graphs the water hammer's duration, pressure and impulse for the same explosion configuration.

Figure 13 shows the extent of bulk cavitation and also the locus of closure. The data for figure 13 resulted from the computer code given in the Appendix. The Appendix' code is an embellishment of the fortran code developed in reference 4. As shown in the Appendix, the code was modified in reference 9 to account for bottom layer acceleration, and modified for the present report to account for afterflow (10).

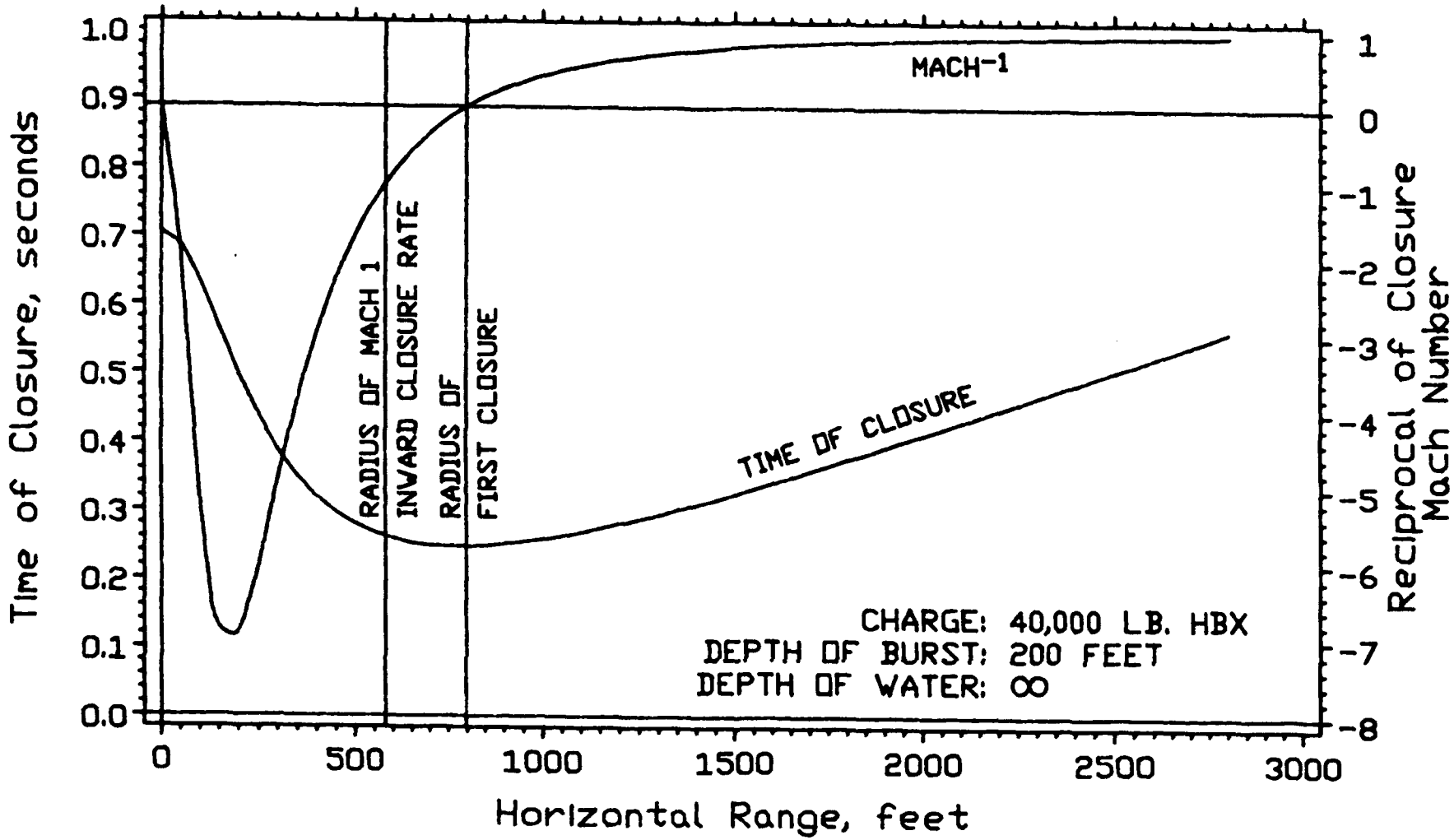

Figure 11. Closure mach number and time of closure for spherical explosion.

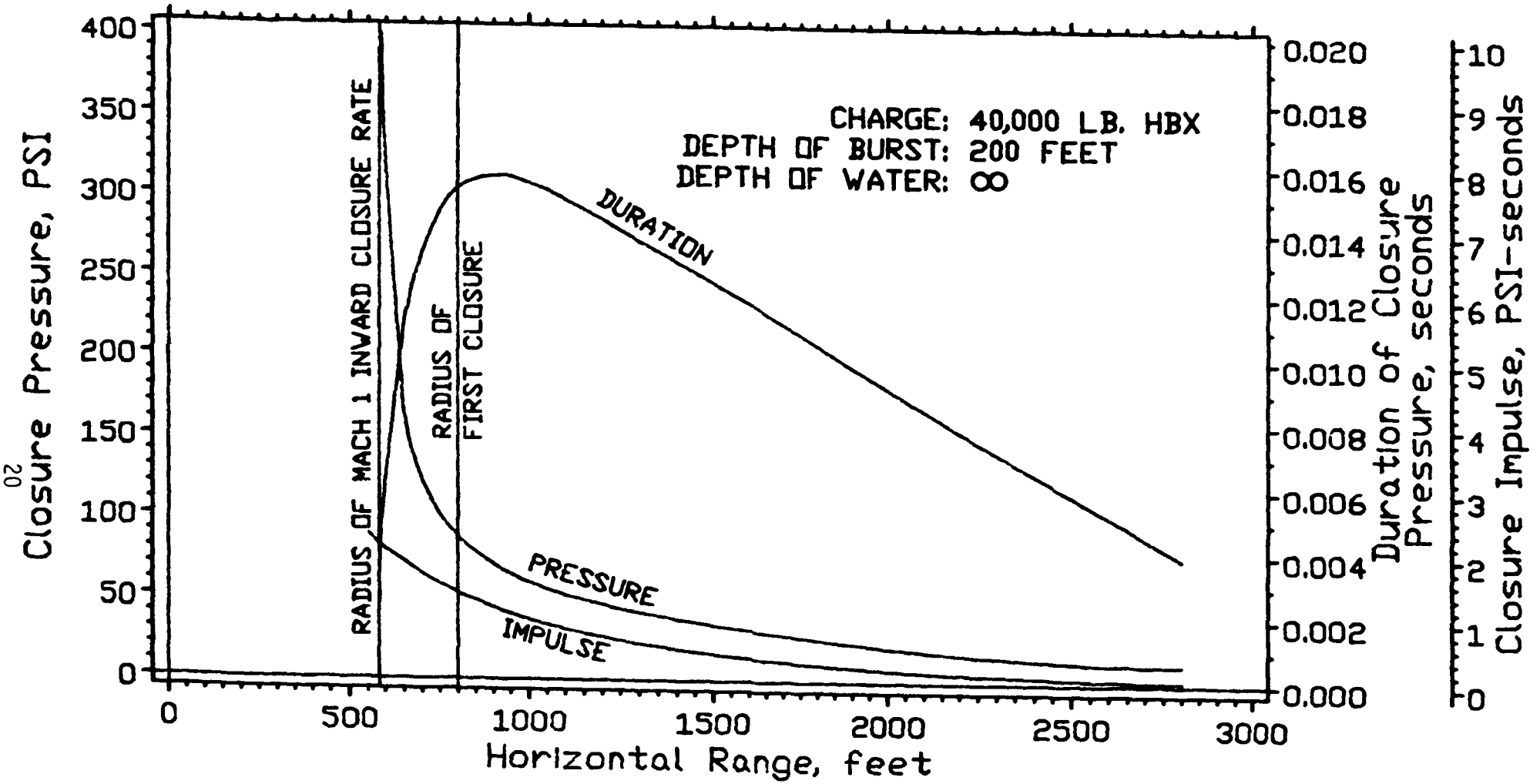

Figure 12. Water hammer's duration, pressure and impulse for spherical explosion.

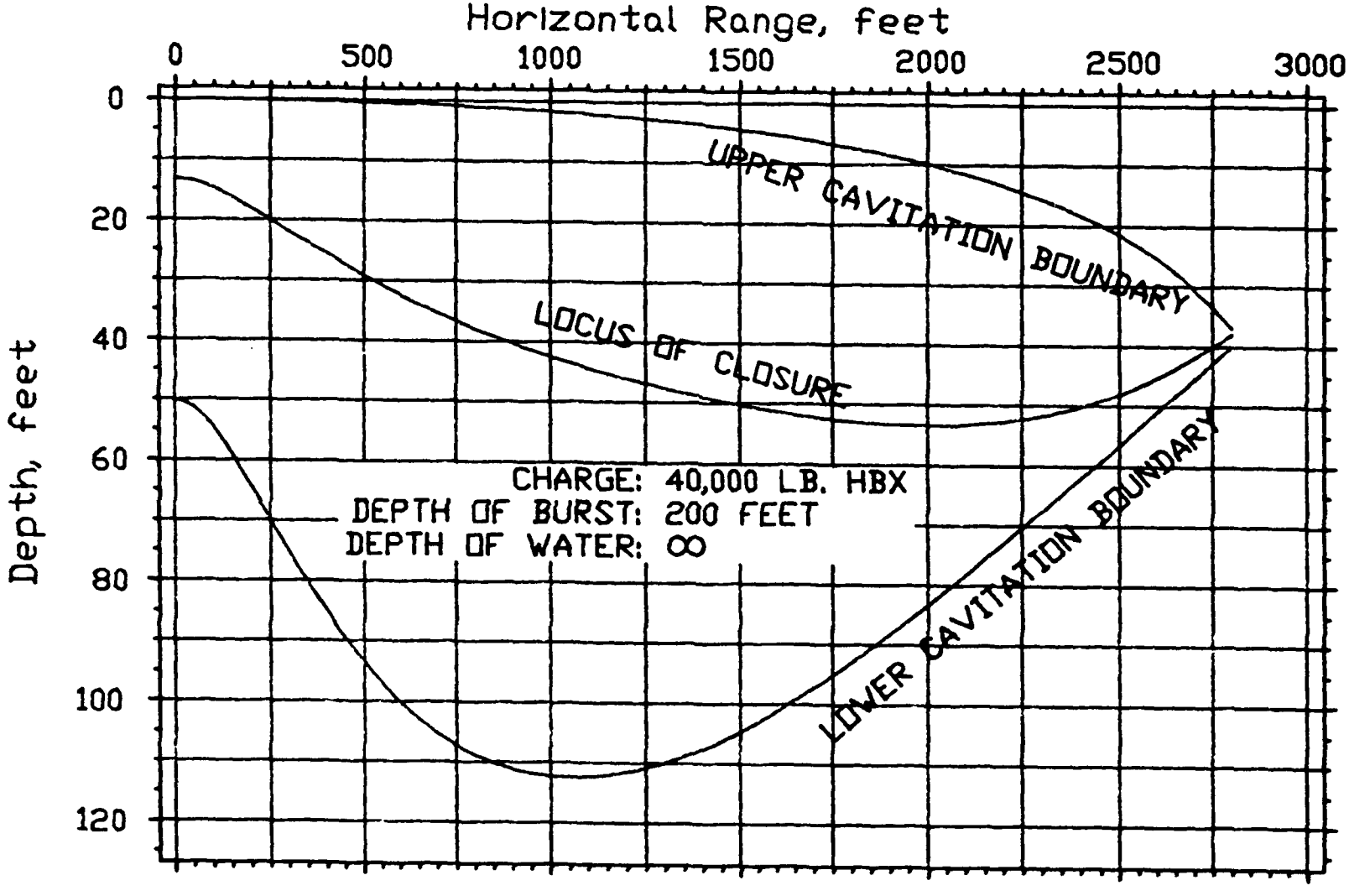

Figure 13. Extent of bulk cavitation and locus of closure for spherical explosion.

SECTION 4

EXPERIMENTAL DATA

4.1 FIELD TESTS.

There have been three field tests specifically designed to investigate bulk cavitation. The first was conducted at UERD in 1962 and reported by Walker and Gorden (ref 47). Theoretical interpretation of its data has been good — until arrival of the first bottom reflections. Thereafter data seems to be the superposition of confusing reverberations.

The second set consisted of the NOL Tests at Mono Lake conducted in 1969 (ref 43). Again, they produced data agreeing reasonably with theory during early times. The Mono Lake tests placed floats with a seismic-suspension integrating accelerometer to measure surface velocity. Figure 14 shows typical results. The integrating accelerometer displayed excessive integration drift about 70 msec after onset of motion.

Data from the Mono Lake tests must be used judiciously owing to unusual sound propagation behavior associated with 1) high salt concentration; 2) substantial concentration of brine shrimp.

The third and more recent tests were conducted by NRL and UERD. They included a more recently developed capability to place PV gages under water — providing useful correlations between pressure and particle velocity throughout the field.

Bulk Cavitation theories do not accommodate bottom reflection (discussed in Section 5). If there is to be a full understanding of Bulk Cavitation it will be necessary to have data from at least one test in deep water, where measurements are not confounded early on by bottom reflections. Enough depth is needed to make sure that a complete cycle of bulk cavitation — incident pressure, generation of cavitation, closure, and measurement of secondary waves — is completed before arrival of the bottom reflection.

4.2 LABORATORY TESTS.

Laboratory tests were carried out in 1969 using an exploding wire as the explosive source [39]. HE tests produce a gas bubble consisting of HE combustion products, whereas the exploding wire is nuclear-like in that it generates a steam bubble.

The facility's original use was to gather information on bulk cavitation. It was later put to use to study (1) shockwave/hull-plate interaction with and without local cavitation, and (2) surface wave generation.

The facility is shown in figure 15. The test vessel is a steel cylinder 6 feet in diameter, with near hemispherical ends to permit vacuum or pressurization to 30 psig. The interior is lined with anechoic material.

The principal observation windows are diametrically opposite, 12 inches in diameter

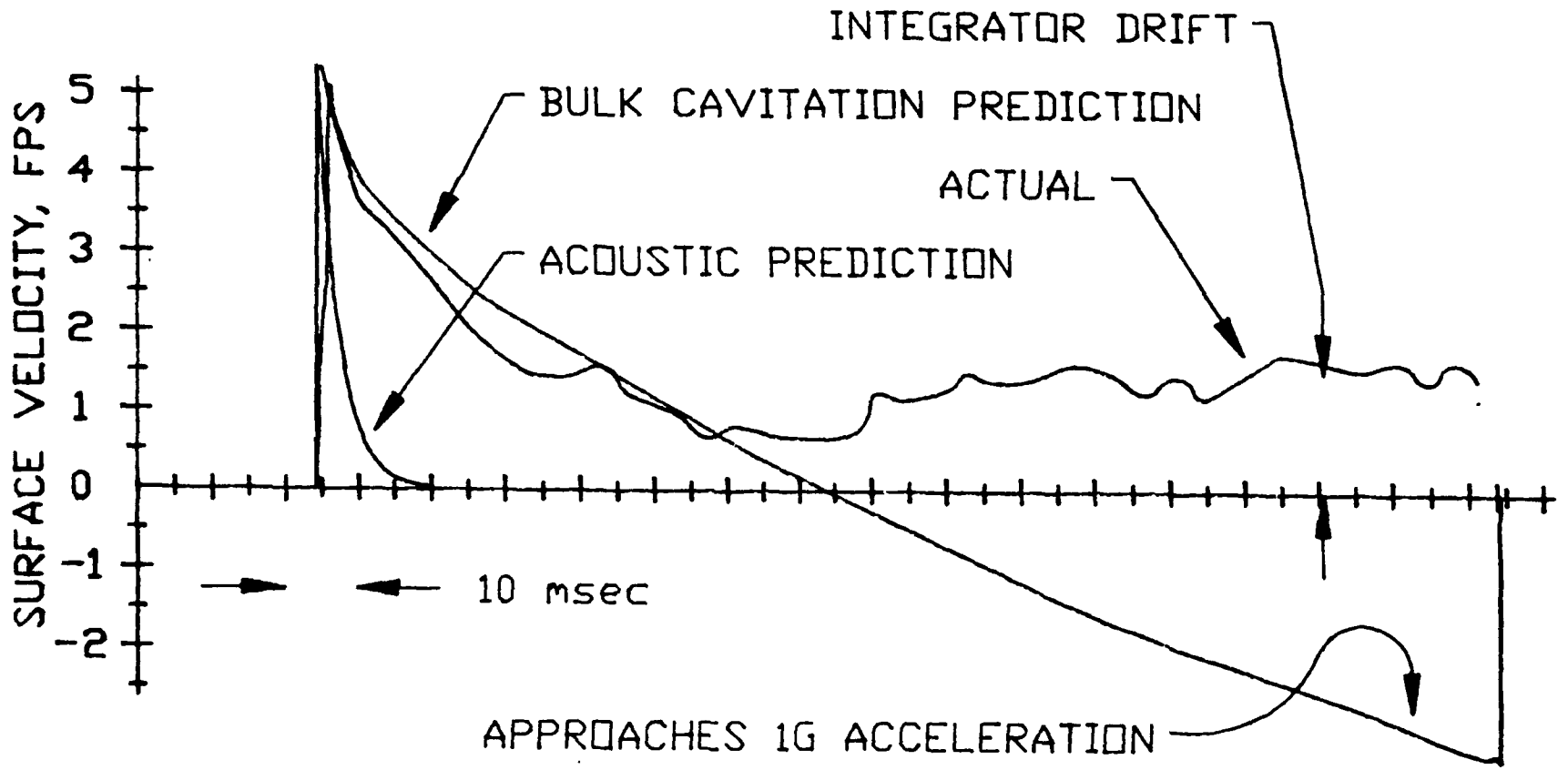

Figure 14. Spall surface velocity in bulk cavitation field test at Mono Lake, 1969.

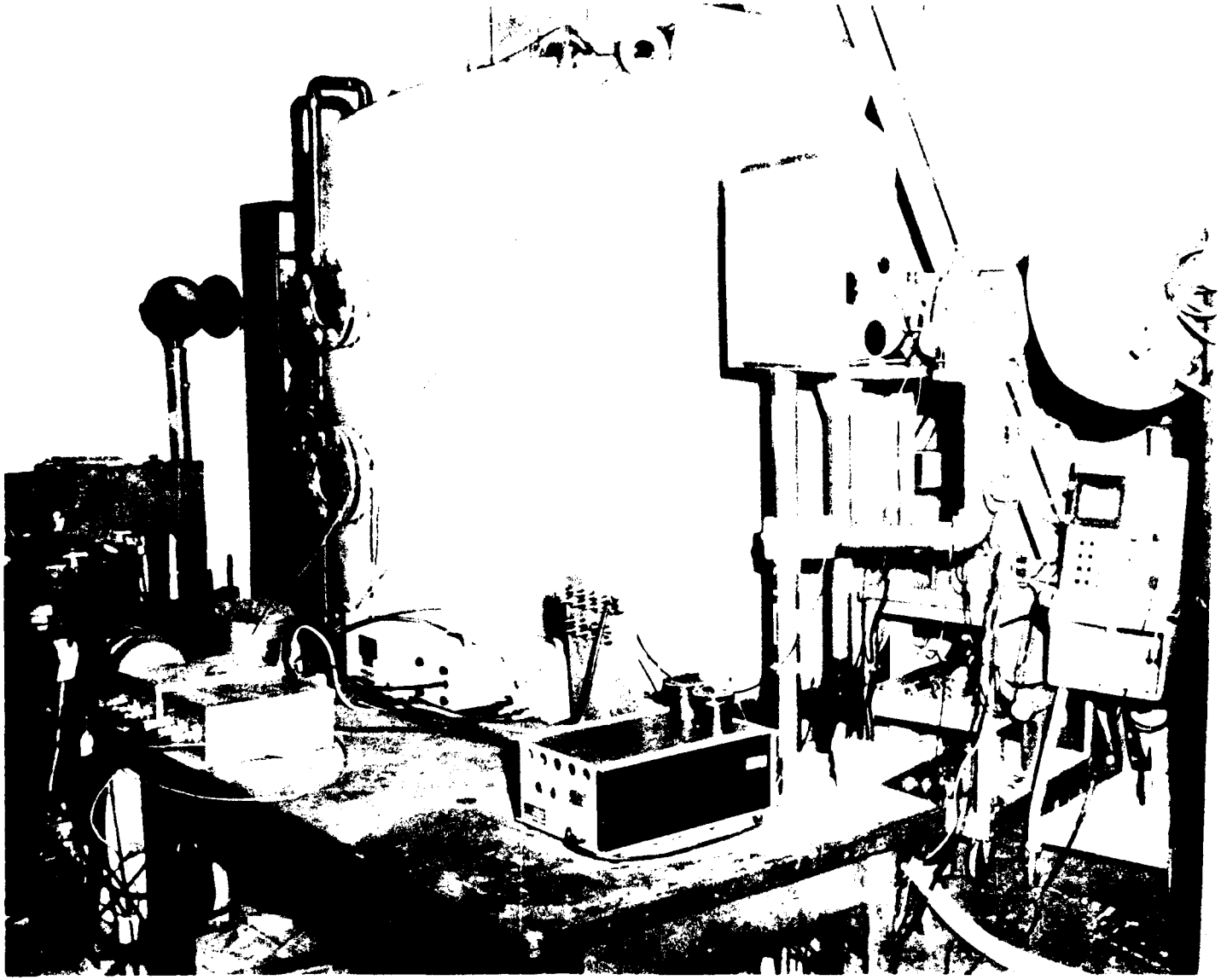

Figure 15. Laboratory explosion test facility using exploding wire to simulate nuclear explosion steam bubble.

and consist of schlierin-free glass. One such window is shown in figure 16.

Depending on application, either schlierin or shadowgraph photos are taken. Light sources available are (a) a 1 μsec spark, (b) a 1 msec xenon flashlamp, and (c) a steady high pressure mercury arc lamp.

The cameras for schlierin work are a single frame 4 X 5 camera as well as a drum camera taking 224 images with frame separation of 40 μsec and shutter speed of 1 μsec. Figure 17 shows a typical sequence of drum camera photos.

For longer sequence durations a 35 mm Fastax camera was used — with frame rates up to 3000/sec. A 16 mm Bolex was also available for very long events.

Miniature piezoelectric hydrophones are used to gather simultaneous pressure-time information.

Energy for the explosion was provided by a 20-KV, 15-μF, 5-nH capacitor. The exploding wire can be positioned anywhere in the tank — above or below the water surface. A 2 mm length of 40AWG nichrome was typically used — virtually a point source for most applications.

The 'nuclear' yield of the exploding wire was of the order of 0.04 gm of TNT. Data analysis showed scaling laws applied favorably over a very wide range — for full scale nuclear (CROSSROADS-Baker, at the same scaled depth of burst in shallow water), large HE (to 10^4 lbs of TNT) and small HE charges (to 10^{-4} lbs of TNT).[28]

With the exploding wire as a simulator for nuclear explosions, the schlierin optics show the progress of direct and reflected shock waves in the water and the air and permit observation of bottom effects and surface effects. Data connecting the generation of surface waves, plumes and air blast have been obtained at low cost. A variety of reflecting bottoms — in material and contour — can be studied.

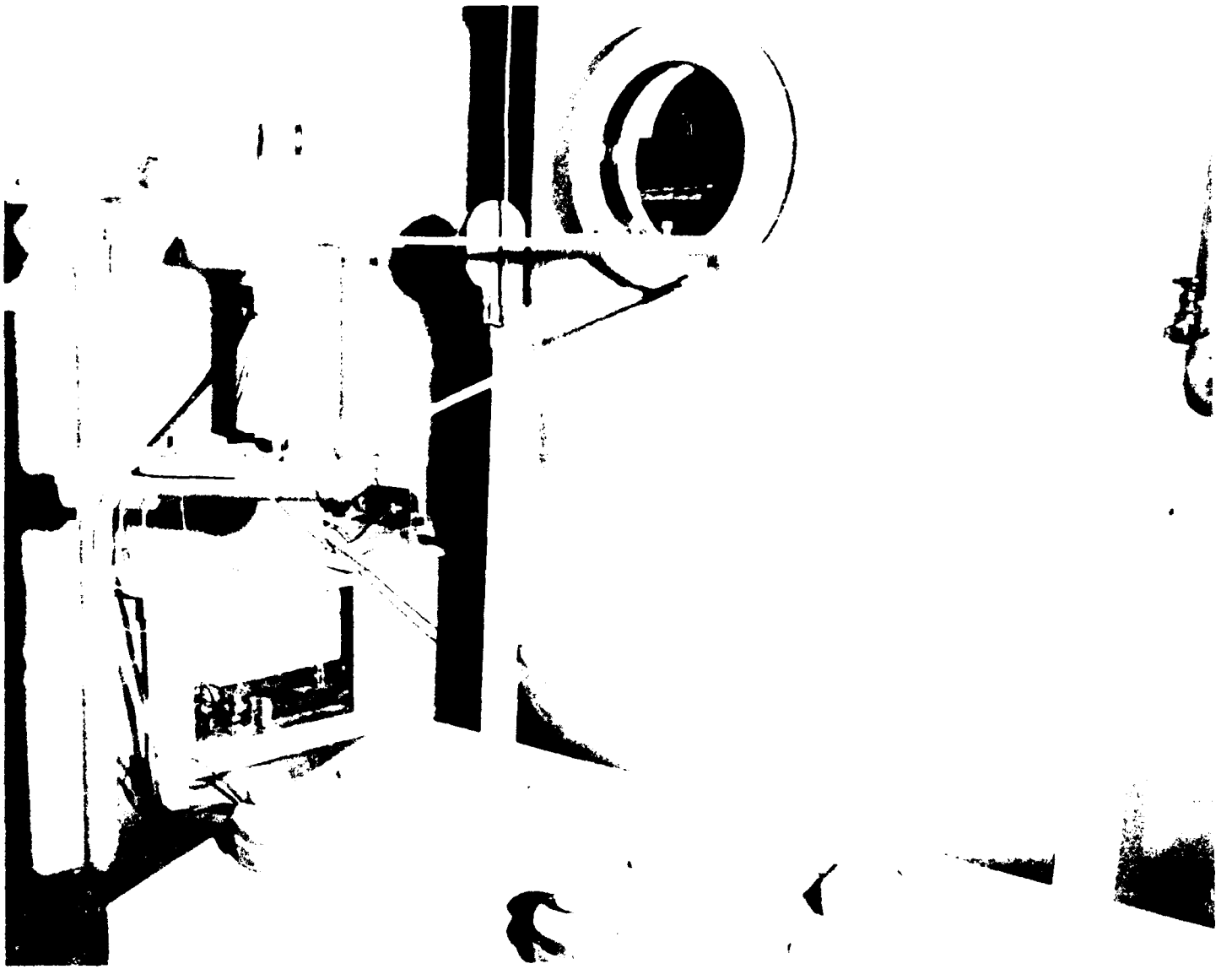

Figure 16. Exploding wire test facility showing one of the schlieren-free observation windows.

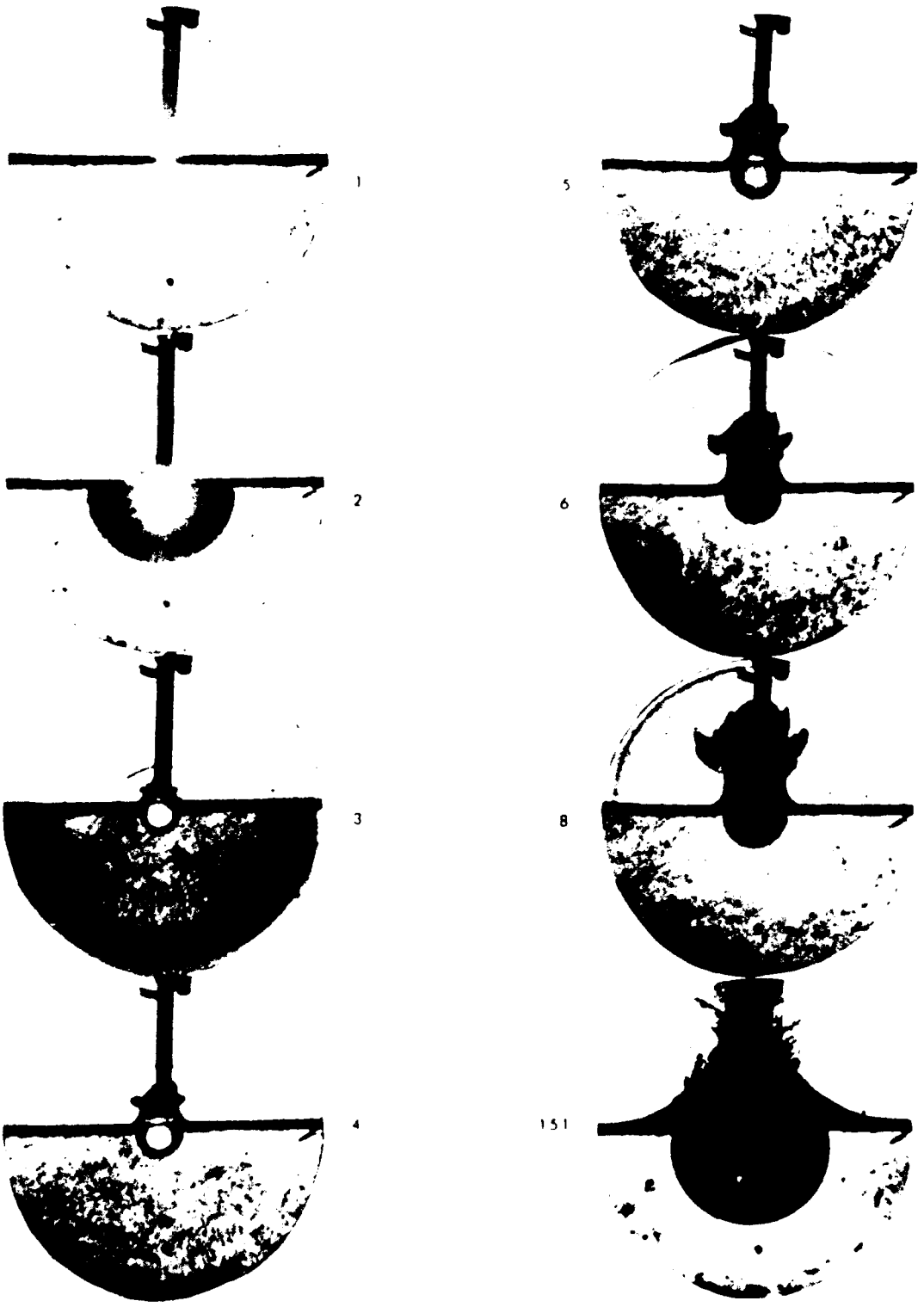

Figure 17. Sequence of drum camera photos taken in exploding wire test facility.

SECTION 5

BOTTOM REFLECTION

5.1 THEORY.

Officer[35] is a good source of information on acoustic bottom reflection. Figures 18 through 21 are interesting excerpts. Figure 18 shows the geometry for explosive source, bottom and receiver. ρ is the density of the medium and c is the speed of sound. For incidence angles less than the critical, θ_c, the reflection coefficient is less than 100 percent, i.e., there is some energy transmitted into the bottom. Beyond the critical angle there is total reflection.

Fig. 19 shows an example of the reflectivity coefficient and phase change α as a function of incidence angle θ — for sinusoidal sound trains. The curves are typical for the usual bottom condition where $c_2 > c_1$ and $\rho_2 c_2 > \rho_1 c_1$ — where c_1 and c_2 are the sound speeds in water and in the bottom respectively, and $\rho_1 c_1$ and $\rho_2 c_2$ are the respective acoustic impedances in these media. In such cases reflectivity reaches 100 percent at some critical incidence angle θ_c; for greater angles the reflectivity remains at 100 percent while the phase α of the wave train begins to shift — reaching 180° phase shift at grazing incidence, $\theta = 90°$.

Such phase shifting causes distortion of an incident wave. For the practical case of a wave with a shock rise followed by an exponential-like decay, reference 2 describes the distortion for angles of incidence beyond the critical, as shown in figure 20. (N.B, the angle α shown in figure 20 is the phase change angle, which is related to the angle of incidence θ as typically shown in figure 19.) The phase angle remains zero — and the wave is undistorted — from normal incidence all the way to the critical incidence angle. Thereafter the phase begins to shift and the wave distortion is as shown in figure 20.

When the phase shift is larger than about 90° for this explosion-like wave shape, one observes a compressive precursor (for times $t < 0$), and a rarefaction follow-up — and these are for for bottom incidence angles generally encountered in underwater explosion tests. This may explain the 'strange' bottom reflection rarefactions noted in Walker and Gordon's 1962 tests.

Friedlander[19] provides theoretical treatment of explosion-like pulses. Figure 21 shows his treatment of a spherical pulse reflecting from a bottom. Reflection front B is for less than critical angle; front L is at the critical angle. Front LEN is beyond the critical angle. For example, along the line ED, we have (1) a gradual rise compressive precursor (compare Figure 20) between E and the 'reflected front' and (2) between the reflected front and D there is a main wave, compressive or rarefactive (compare Fig. 20). LEN is an unequivocal precursor for that portion beyond the incident, near N.

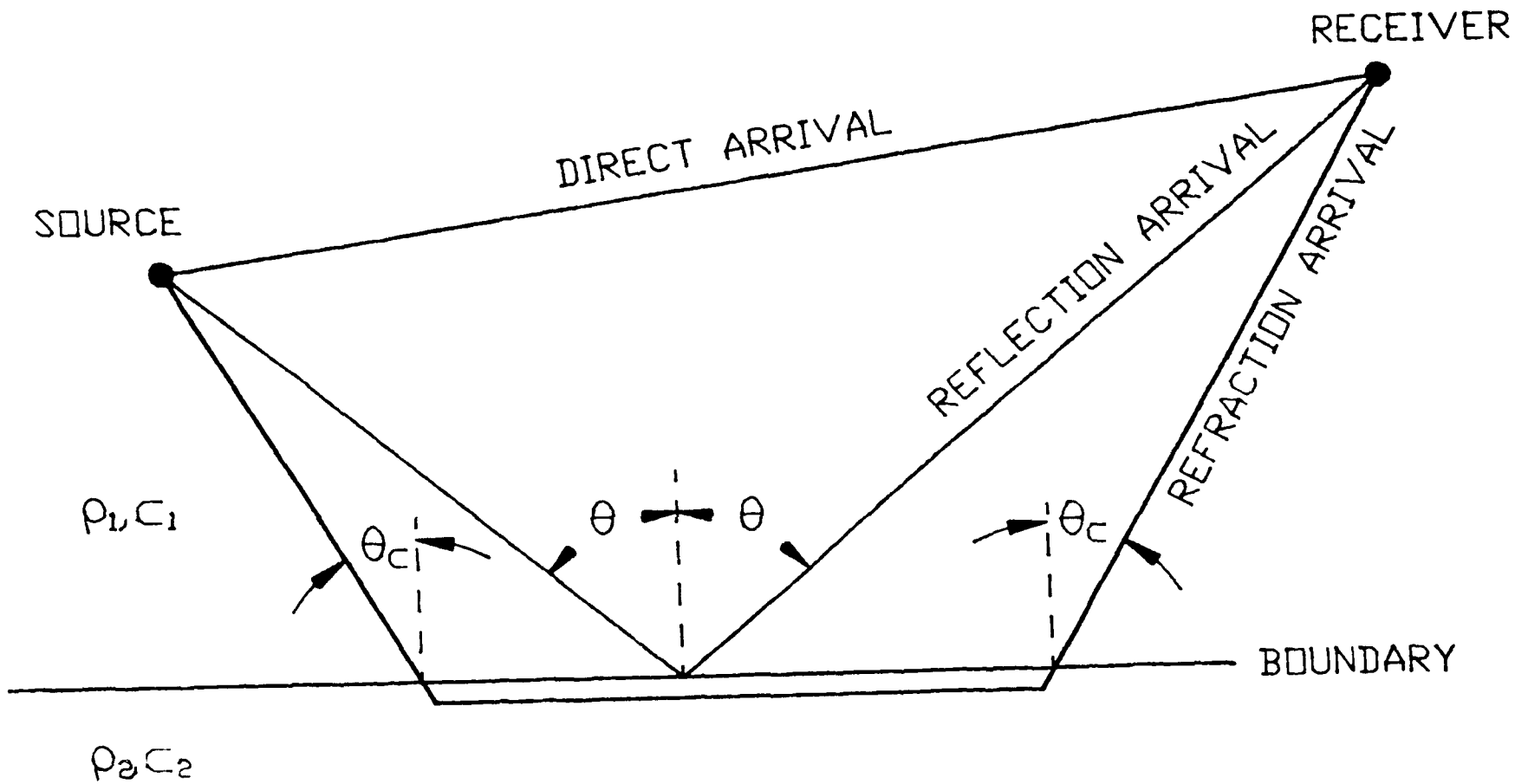

Figure 18. Bottom reflection geometry, showing explosive source, bottom and receiver.

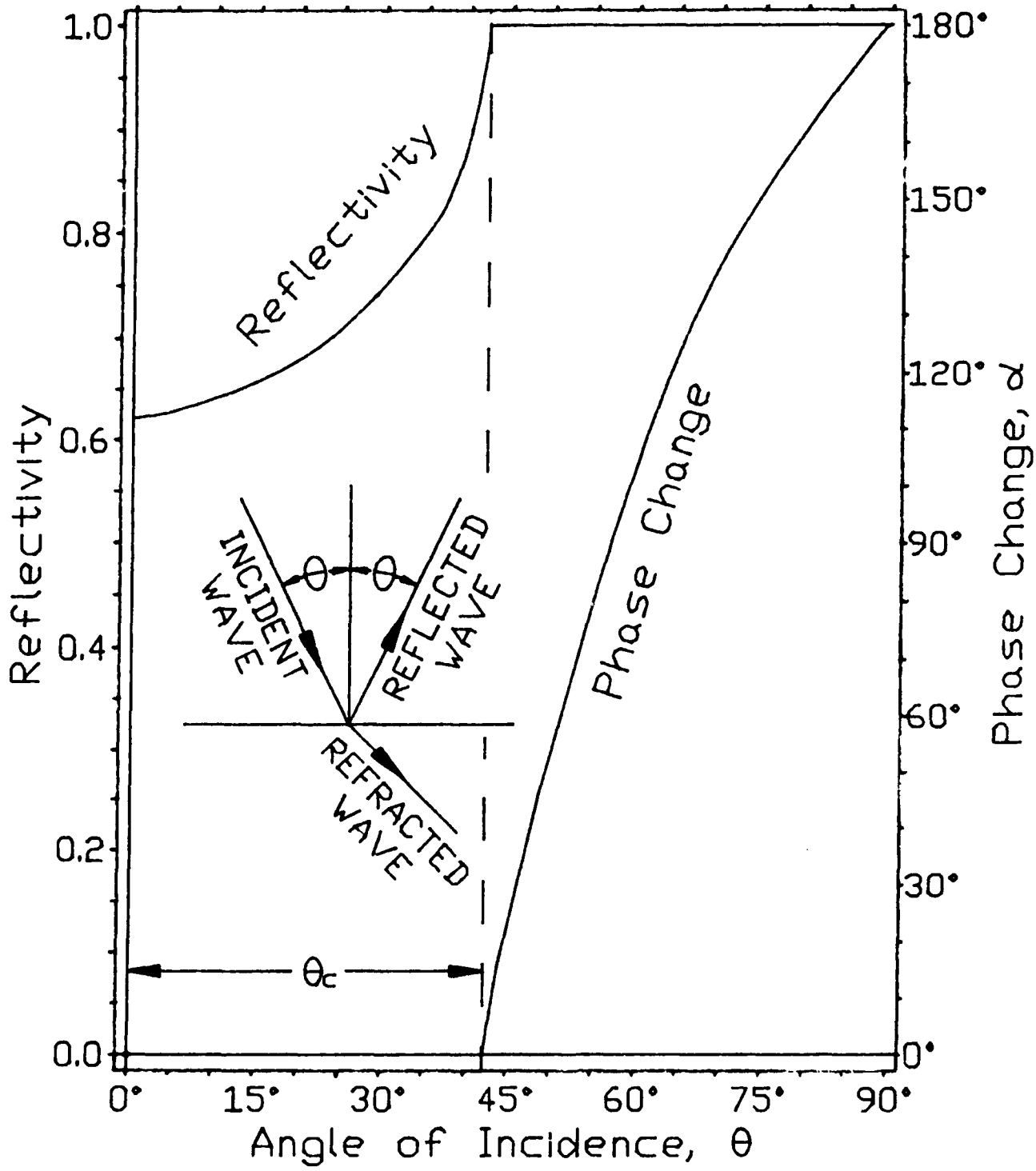

Figure 19. Phase change α and reflectivity coefficient as a function of incidence angle θ — for sinusoidal sound trains.

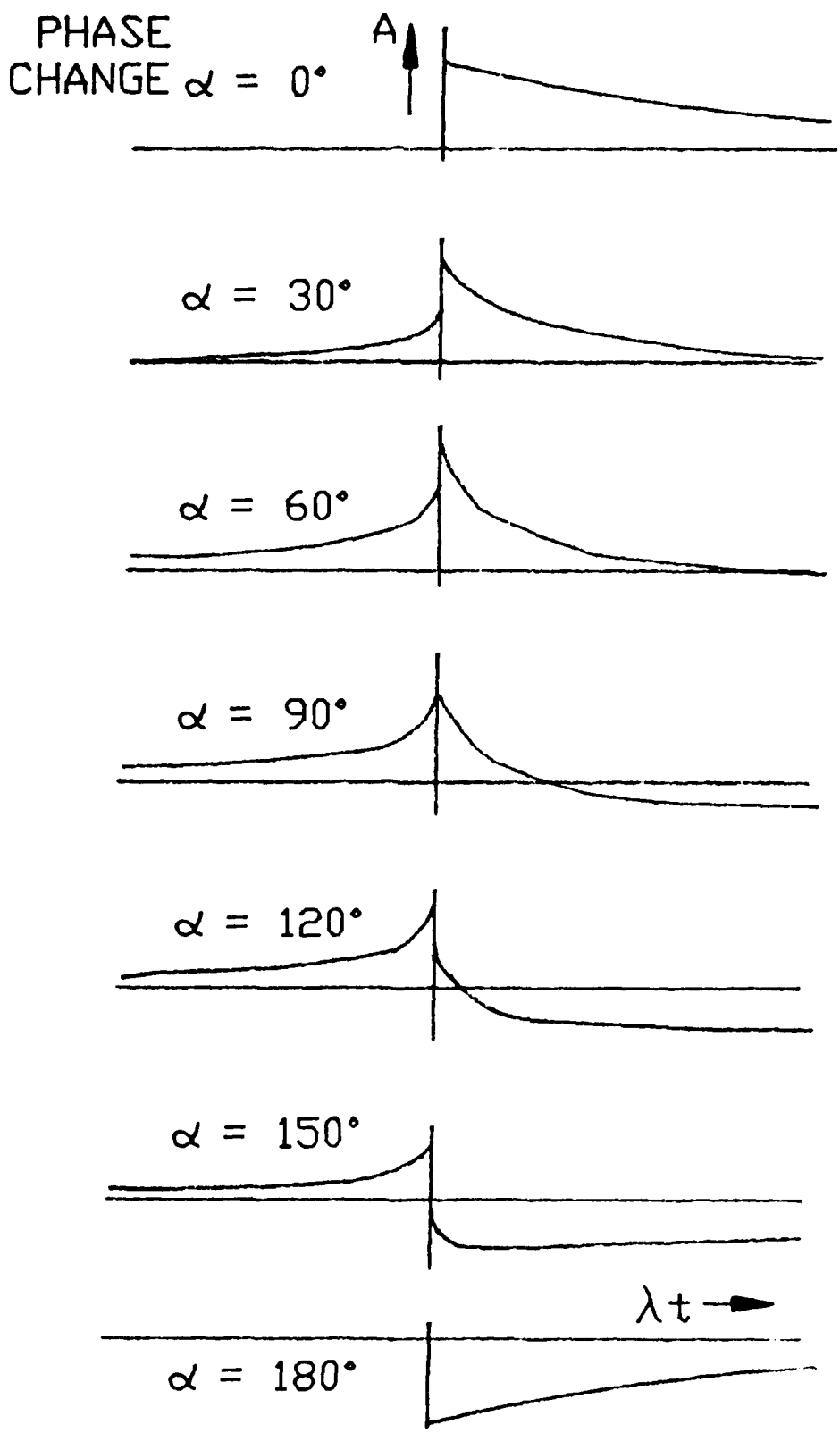

Figure 20. Wave distortion for incidence angles beyond the critical.

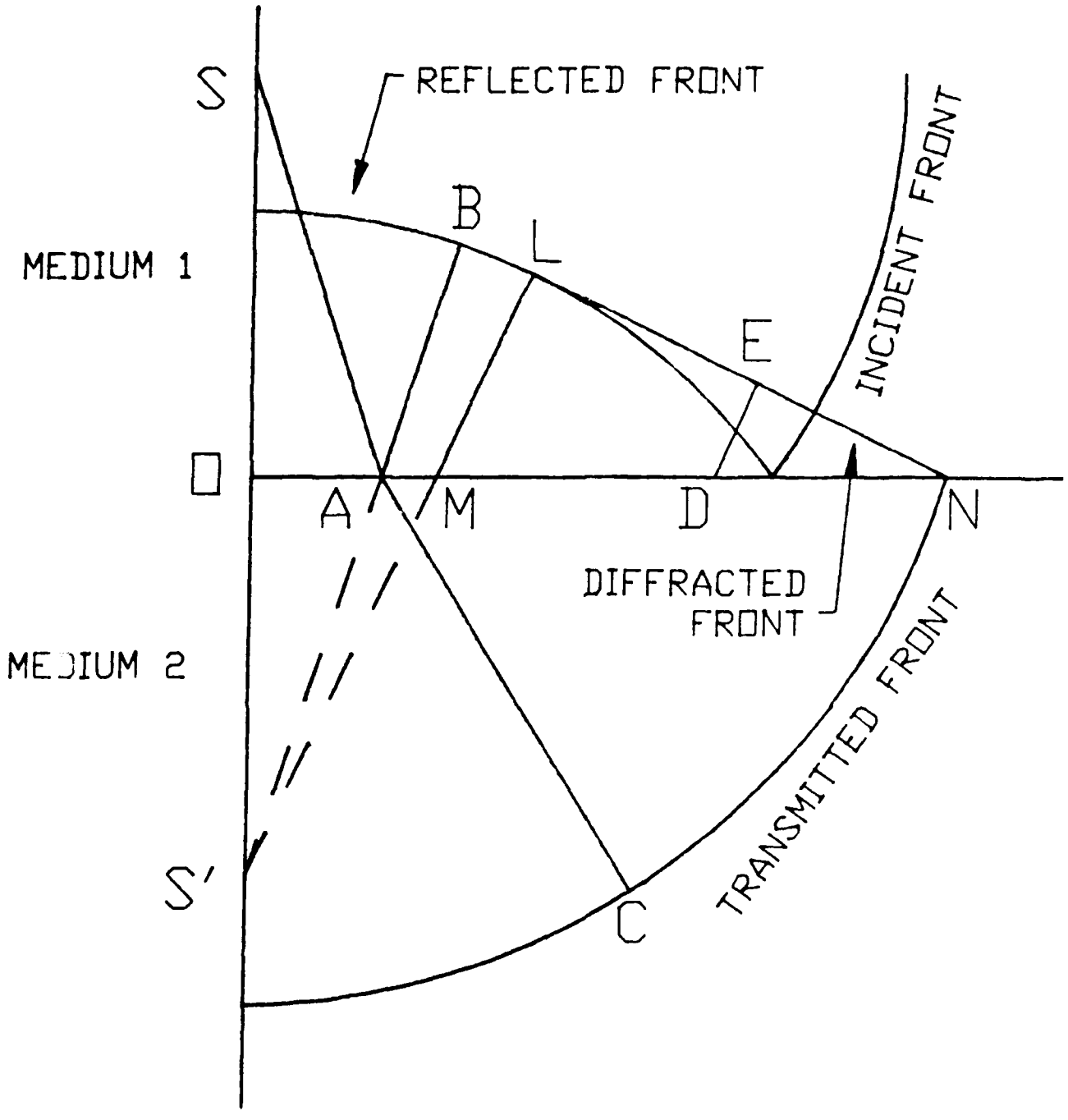

Figure 21. Friedlander's treatment of spherical pulse reflecting from bottom.

5.2 SHOCK TESTING CONSIDERATIONS.

Bottom reflections can play a significant role in shock testing. Lacking adequate knowledge of bottom conditions, one must meantime consider what can happen with 100 percent reflection, coupled with bulk cavitation effects.

Among the test configurations considered was the following:

Explosive weight:	40,000 lbs HBX
Explosive depth:	200 feet
Water depth:	700 feet
Horizontal Range:	722 feet

Using the analysis of reference 15 (embodied in the program listed in the Appendix), at a horizontal range of 722 feet the bottom reflected wave would appear to cause a second round of bulk cavitation (beginning just after closure of the first cavitation). The impact velocity — and consequent closure hammer pressure — is larger than that of the first cavitation closure. Further, the geometry is such that the second cavitation closure first occurs at a horizontal range of 1800 feet; however, the mach 1 closure point — where peak pressure increases without bound — occurs at a horizontal range of 720 feet.

At a horizontal range of 722 feet, the surface incidence angle of the main shock is about 75°. The surface incidence angle of the bottom reflection is about 30°. Even though the reflected pressure is only half (assuming unity bottom reflectivity) of the main pressure, the change in incident angle more than compensates, generating higher spall velocity and consequently higher closure hammer velocity.

Figure 22 shows the expected pressure history at a depth of 21 feet and horizontal range of 722 feet. The second cavitation closure pressure is theoretically infinite; however, the impulse is finite, estimated to be about 3 psi-seconds (compared with a value of 0.92 for the impulse owing to closure of the first cavitation).

Without adequate knowledge of bottom conditions in proposed shock testing it is not possible to predict whether or not there might be a surprisingly large impulse delivered owing to interaction of bottom reflection and bulk cavitation.

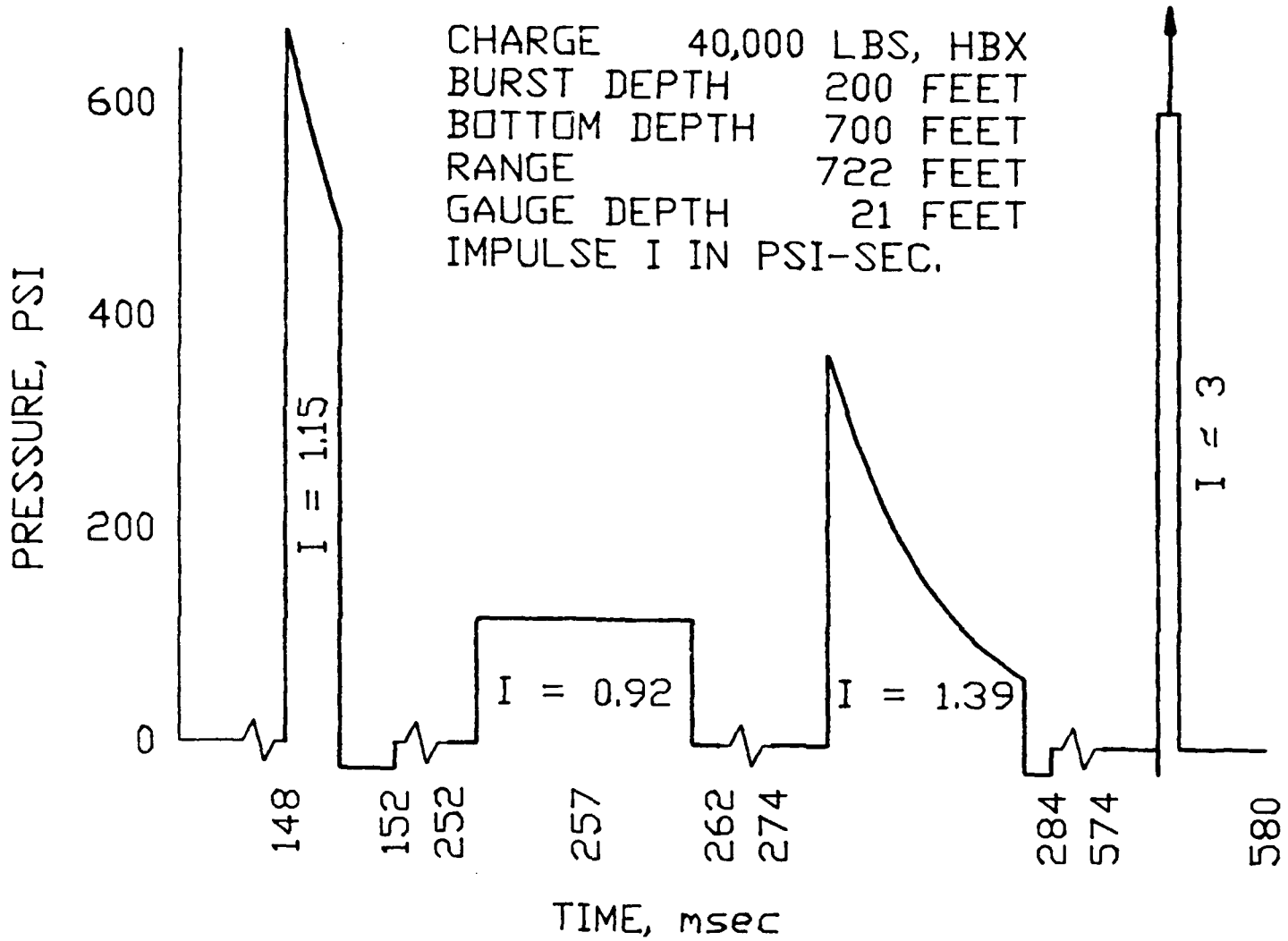

Figure 22. Possible expected pressure history for shock test of ship.

SECTION 6

HULL PLATE LOADING

A prime concern for underwater shockwave/ship interaction is the effects on equipment within a ship. Secondly, observed hull plate buckling is enough to cause flow noise that compromises a ship's sonar ability. The mechanisms of hull plate buckling are not adequately understood.

Analytical solutions to the problem were first sought during WWII.[25,27,31,45] Tests and analysis pointed to local cavitation playing a major role. The underwater Explosives Research Division of NSRDC conducted a number of HE tests during the 1960s to study the mechanisms of hull damage from underwater explosions. At that time it was realized that there were three intertwined phenomena contributing to hull plate damage: (1) initial shockwave/hull-plate interaction, (2) local (and perhaps also bulk) cavitation and closure, and (3) diffraction.

The complexity requires machine numerical methods. Even so, a semi-quantitative analysis — not involving diffraction — enabled interpretation of the UERD data.[12]

Though no analytical solution is available, the differential equations representing the problem can be set up and solved digitally. Useful results have been obtained by a number of workers for the situation where the water is always an acoustic medium, i.e, at depth where ambient pressure allows large negative acoustic pressures.[4,6,17,21,-22,23,29,36]

More recent numerical treatment includes provision for a bilinear acoustic medium interacting with simplified structural configurations.[5,18,33,34,37]

Original insights into hull plate loading stylized the interaction to be that of shockwave and plate.[45] Late time effects in these analyses pointed toward local cavitation as a major affect[25]. Afterflow was also considered as a late time loading mechanism.[41]

6.1 OBSERVATIONS

Streak camera tests have been conducted on a circular diaphragm — held on a test hull bottom by a heavy rim — and subjected to an HE shockwave.[24] The results are summarily sketched in figure 23. The first sketch shows the diaphragm immediately after it has been struck by the shock front — it has just begun to move. The space between the diaphragm and the reflected shock front has been expanded in the adjacent box which shows the pressure distribution. There, we see that the reflected shock front is moving into the waning portions of the initial, incoming shockwave. The sum of pressures in the incident wave and the reflected wave cause substantially a pressure doubling.

As the diaphragm accelerates to higher velocity, the reflected wave, initially a compression, becomes increasingly rarefactive. In the pressure distribution box, we therefore observe the rapidly decreasing total pressure. If water could withstand tension, the total pressure would follow the dotted line. However, it cannot; hence, near the

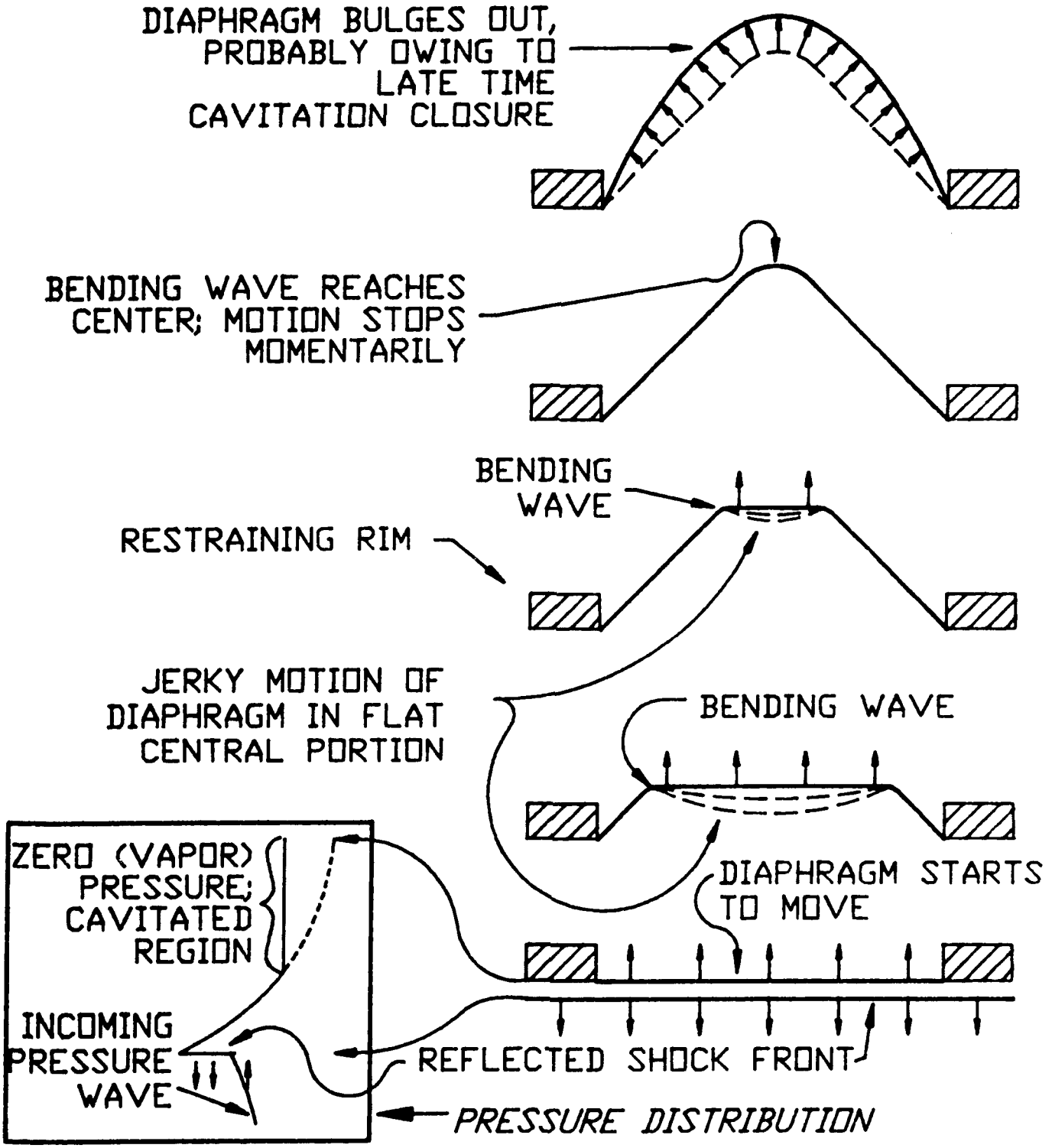

Figure 23. Summary of streak camera tests showing response of circular diaphragm to incident shockwave.

diaphragm the water cavitates — by forming vapor bubbles, or by forming water droplets in a matrix of water vapor. Whichever way, the pressure in the cavitated region is that of water vapor, effectively zero for our purposes.

Sketch 2 shows the diaphragm at a later time. The flat central portion of the diaphragm does not yet know that the edges have been clamped by the heavy rim; a bending wave, travelling inward, carries this information. The streak camera record displays a jerky motion as shown in the second and later sketches. Theoretical work has not shown a cause for this jerkiness. It is conjectured that a water layer, still attached to the diaphragm, is vibrating.

Later sketches show further motion and progress of the bending wave. Next to last sketch shows the bending wave reaching the center. The camera record indicates that all motion has momentarily stopped.

Then, at a substantially later time, the diaphragm is bulged outward. It appears that this late impulse is a water hammer that takes place at cavitation closure.

6.2 PRELIMINARY ANALYSIS.

Kennard has displayed the physics of shockwave/hull interaction involved quite well by a variety of analytical treatments with restricting assumptions.[27]

Four characteristic times are used (see figure 24b):

1. t_w wave time — the incident wave is assumed for analytical purposes to have a shock rise to pressure p_o followed by exponential decay with time constant t_w.
2. t_m maximum time — required for the hull structure being analyzed to reach maximum velocity.
3. t_d diffraction time — the time required for an underwater acoustic wave to propagate from the structure's center to its edge.
4. t_s swing time — the time required for the structure to reach maximum deflection and come to rest.

The simplest analysis showing hull/cavitation phenomena is that of an exponential-like shock wave striking a plate of infinite lateral extent, as shown in figure 24a.[27,45]

If the areal density of the plate is m, a damping time constant t_p comes into play, defined by

$$t_p = m/\rho c \quad . \tag{7}$$

t_p may be visualized as the time required for a sound wave to traverse a thickness of water having the same mass as the plate.[27] For example, a one-inch steel plate has a damping time of 0.129 msec; a rigid hull drawing 30 feet of water has an effective damping time of 6 msec (for a wave shocking it from the bottom).

In figure 24a we see the incident shock wave. At any instant at the plate the incident plus reflected shock wave sum to a pressure doubling, i.e, a pressure of $2p_i$.

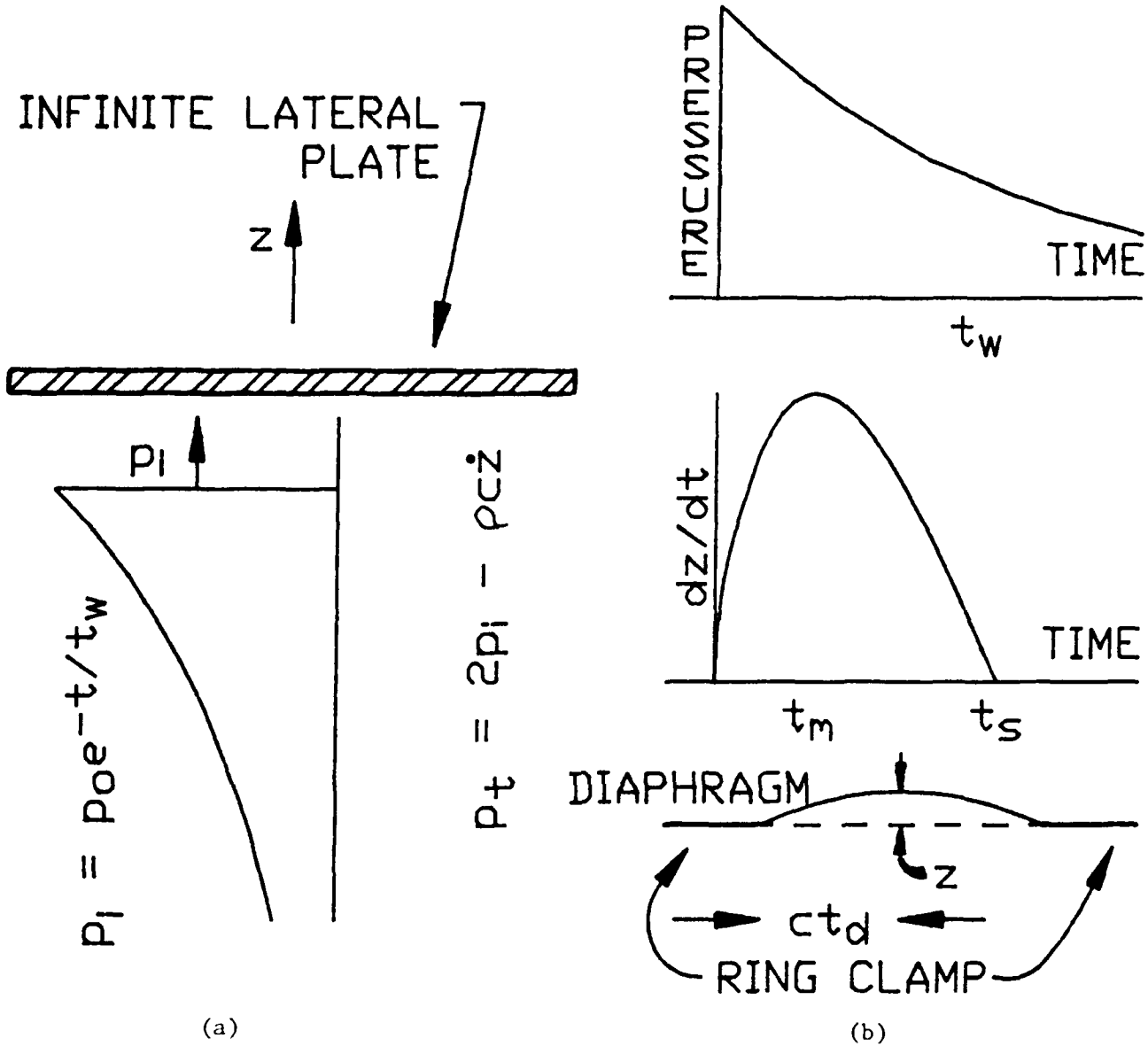

Figure 24. (a) Exponential-like shockwave incident on plate of infinite lateral extent.
(b) Characteristic times employed in analysis of shocked plate.

Superposed on this is a rarefaction wave owing to motion of the plate. As indicated in figure 24a, the magnitude of the rarefaction is $\rho c \cdot dz/dt$ -- where ρ is the water density (65 lbs/ft^3 or 2 slugs/ft^3), c is the speed of sound in water (5000 fps), and z is the displacement of the plate. ρc is the acoustic impedance of water.

The equation of motion for the problem shown in figure 24a is

$$m \cdot d^2z/dt^2 = 2p_i - \rho c \cdot dz/dt \quad . \tag{8}$$

The incident shock pressure is described by

$$p_i = p_o e^{-t/t_w} \quad . \tag{9}$$

Wave time t_w and peak pressure p_o follow empirical scaling laws[10]:

$$t_w = MW^{1/3}(R/W^{1/3})^m \quad , \tag{10}$$

$$p_o = K(W^{1/3}/R)^k \quad , \tag{11}$$

where R is the radius from the explosive and the empirical constants are shown in Table 1 for various explosives.[10,11,43]

Table 1

Explosive	K, psi	k	M, msec	m
HBX-1	23,980	1.13	0.0654	0.18
Lithanol	13,180	1.13	0.12	0.18
Pentolite	22,500	1.13	0.0969	0.08
TNT	21,600	1.13	0.0676	0.24

The ensuing graphs of pressure and motion of the shockwave/plate interaction are plotted in terms of the following dimensionless variables:

$$r = t_p/t_w \quad , \tag{12a}$$

$$P_i = p_i/p_o \quad , \tag{12b}$$

$$P_t = p_t/p_o \quad , \tag{12c}$$

$$P_r = P_t - P_r \quad , \tag{12d}$$

$$U = \dot{z}/(p_o/\rho c) \quad , \qquad \text{(plate velocity)} \tag{12e}$$

$$T = t/t_w \quad , \tag{12f}$$

$$KE = \int_o^T P_t \cdot U \cdot dT \quad , \qquad \text{(kinetic energy of plate)} \tag{12g}$$

$$Z = z/\lambda \quad , \tag{12h}$$

where shock wavelength λ is related to t_w by

$$\lambda = c \cdot t_w \quad , \tag{12i}$$

and c is the speed of sound in water.

In terms of these the dimensionless input shockwave is expressed by

$$P_i = e^{-T} \quad , \tag{13a}$$

and the various responses are:

$$P_t = 2[e^{-T/r} - re^{-T}]/(1-r) \quad , \tag{13b}$$

$$P_r = P_t - P_r \quad , \tag{13c}$$

$$U = 2[e^{-T} - e^{-T/r}]/(1-r) \quad . \tag{13d}$$

These are plotted in figure 25 for respective r values of 0, 1/4, 1 and 4.

6.3 LOADING AT DEPTH.

If plate loading takes place at sufficient depth — ambient pressure (atmospheric plus hydrostatic) is large — then the acoustic wave negative pressures are realizeable: the entire plate loading process can be described in terms of the foregoing graphs.

The area under the P_t curve is the impulse imparted to the surface plate. The impulse is maximum at some time T_{to}, depending on the value of the parameter r. Thereafter P_t goes negative and thereby begins decelerating the surface plate; it begins to withdraw impulse from the plate. Indeed if we wait several time constants — let T approach infinity — the acoustic pressures will withdraw all impulse loading from the plate. The plate will come to rest.

Figure 26 shows values of T_{tc} for values of r.

P_t, the reflected pressure, overall has a total (dimensionless) impulse of zero. Hence, the total impulse of P_r is opposite to that of P_i. At depth, then, the reflected pressure can radiate downward to infinity, carrying away energy and momentum, ultimately leaving the plate motionless.

Hence in a totally acoustic plate loading, the maximum impulse (up to a maximum of -2 for large r) is imparted to the plate at time T_{to}. Thereafter the acoustic waves proceed to unload the plate, ultimately: (1) leaving it with zero imparted impulse; (2) delivering all the incident wave's impulse to the reflected wave's impulse, which radiates away to infinity.

6.4 LOADING NEAR THE SURFACE.

If we are not at significant depth — i.e., a vessel at or near the surface — the above described acoustic waves can be followed only up until approximately T_{to}, when the total pressure passes through zero. Thereafter the total acoustic pressure P_t cannot continue into its negative phase; the water ruptures and cavitation takes place.

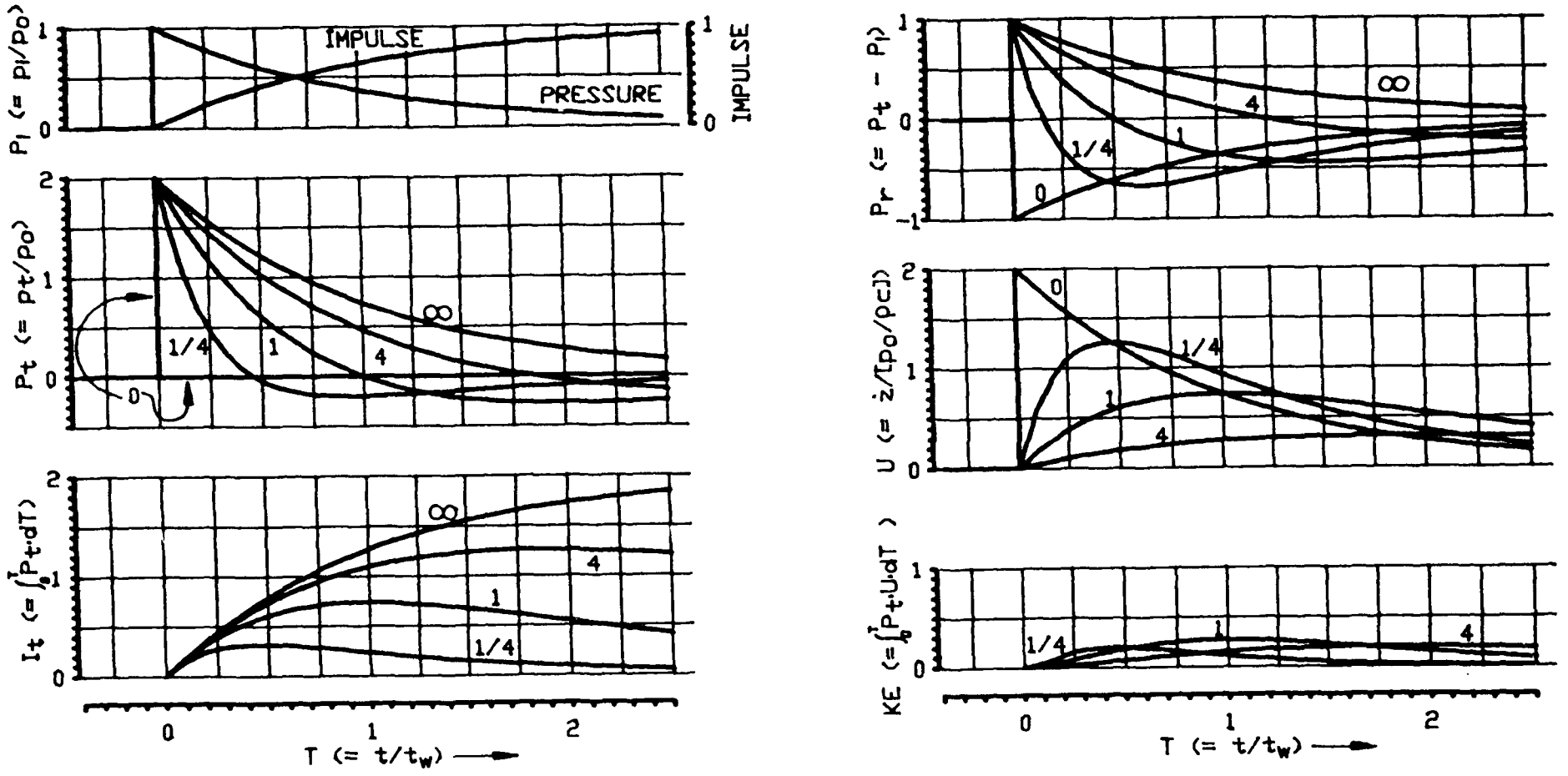

Figure 25. Dimensionless variables as function of time for shocked plate.

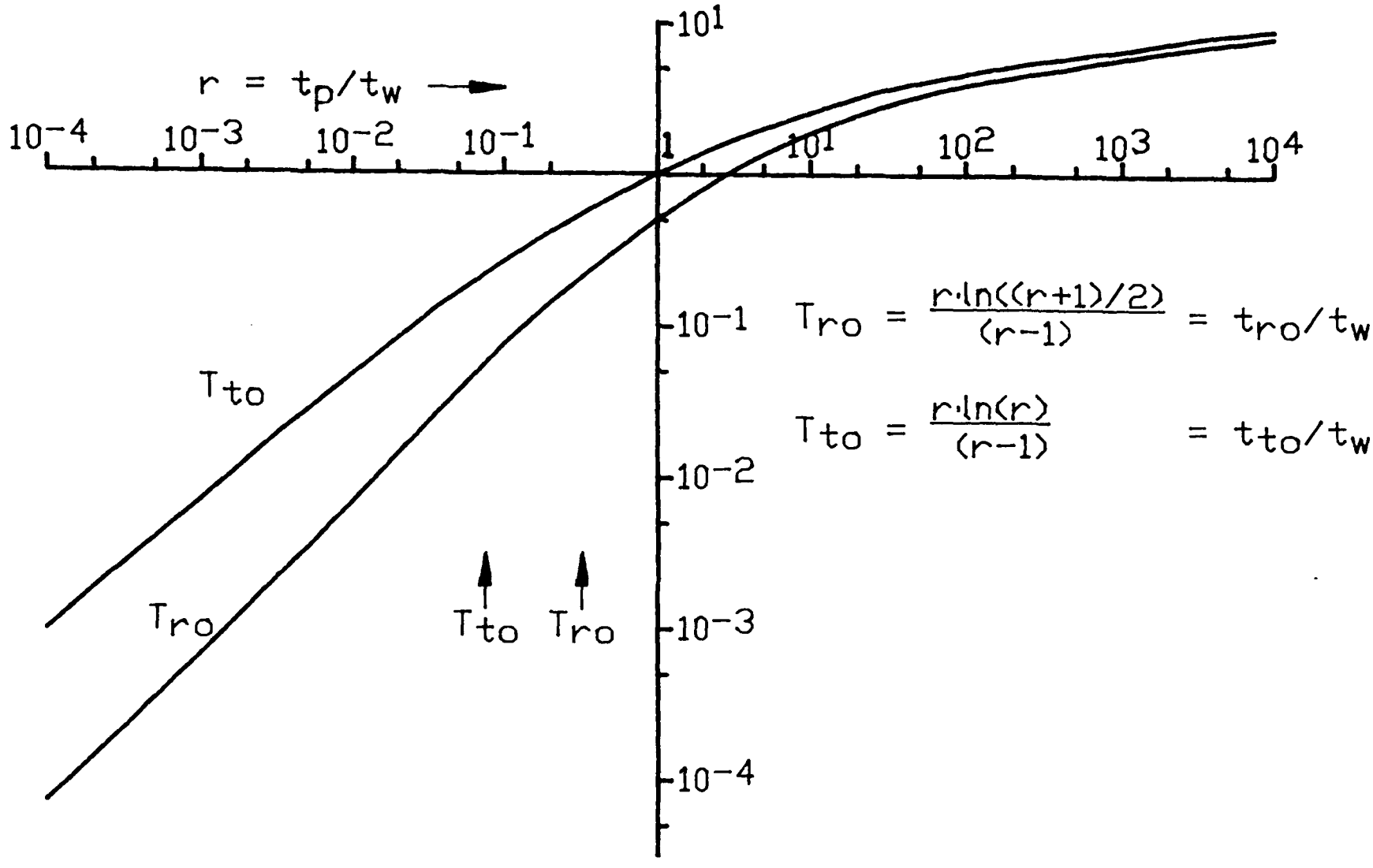

Figure 26. Time of maximum impulse T_{to} and time of reflected wave's zero crossing T_{ro} — for shocked plate.

We can use these acoustic curves to find the condition of the plate at time T_{to}, when the plate has received maximum impulse. After cavitation the actual pressure P_t remains at zero (actually the vapor pressure of water — practically zero); no impulse is subsequently withdrawn from the plate.

By time T_o the reflected wave P_r has become negative. This reflected wave is travelling down into the water; hence, its argument as a travelling wave is T-Z (dimensionless time minus dimensionless displacement). Since this reflected pressure wave $P_r(T-Z)$ is propagating back down into the water, it moves into the waning portions of the incoming $P_i(T+Z)$. Thus at some place and time, $P_r(T-Z)$ plus $P_i(T+Z)$ becomes negative — physically not allowed at shallow depths (where ambient pressure — sum of atmospheric and hydrostatic pressures — is effectively zero); the water cavitates. As time progresses the boundaries of this growing cavitated region are determined by the two values of Z that approximately satisfy, at each time T[11,15,46]

$$P_i(T+Z) + P_r(T-Z) = 0 \ . \tag{14}$$

The only portion of $P_r(T-Z)$ that ultimately escapes the cavitation process is the compressive front, which is seen in figure 25 to end at some time T_{ro}, depending on the value of the parameter r.

Beyond T_{ro} figure 25 shows that the additional impulse in the reflected wave $P_r(T-Z)$ is negative. All of this negative impulse — initially the tail of $P_r(T-Z)$ radiating down away from the plate — cannot escape and ultimately is deposited in a spall of cavitated water beneath the plate.

There are four impulses to consider when the loading and cavitation processes have been completed (but prior to the beginning of the cavitation closure process, i.e., the cavitation closure phase of further loading of the surface plate):

1. I_i - the total impulse of the incident compression wave (equal to unity in dimensionless terms);
2. I_{to} - the total impulse imparted to the surface plate by the reflected wave;
3. I_{ro} - the total impulse (which escapes to infinity) in the compressive front of the reflected wave; and
4. I_s - the total impulse or momentum in the cavitated slug of water immediately beneath the surface plate.

The mathematical definitions of these are shown in figure 27. Momentum conservation requires

$$I_i + I_{to} + I_{ro} + I_s = 0 \ . \tag{15}$$

These impulses, as a function of the time constant ratio r, are graphed in Figure 27. Also shown, in Figure 26, are the pertinent times, T_{to} and T_{ro}, as a function of r.

r is small if (1) the surface load m is sufficiently small (including zero, the situation for Bulk Cavitation), regardless of t_w (i.e., for small or large explosive charges); or, (2) t_w is large (corresponding to large scale HE and nuclear).

For large r cavitation plays no important role - negligible incident impulse is deposited in a cavitated spall — cavitation is effectively nonexistent. Behavior is

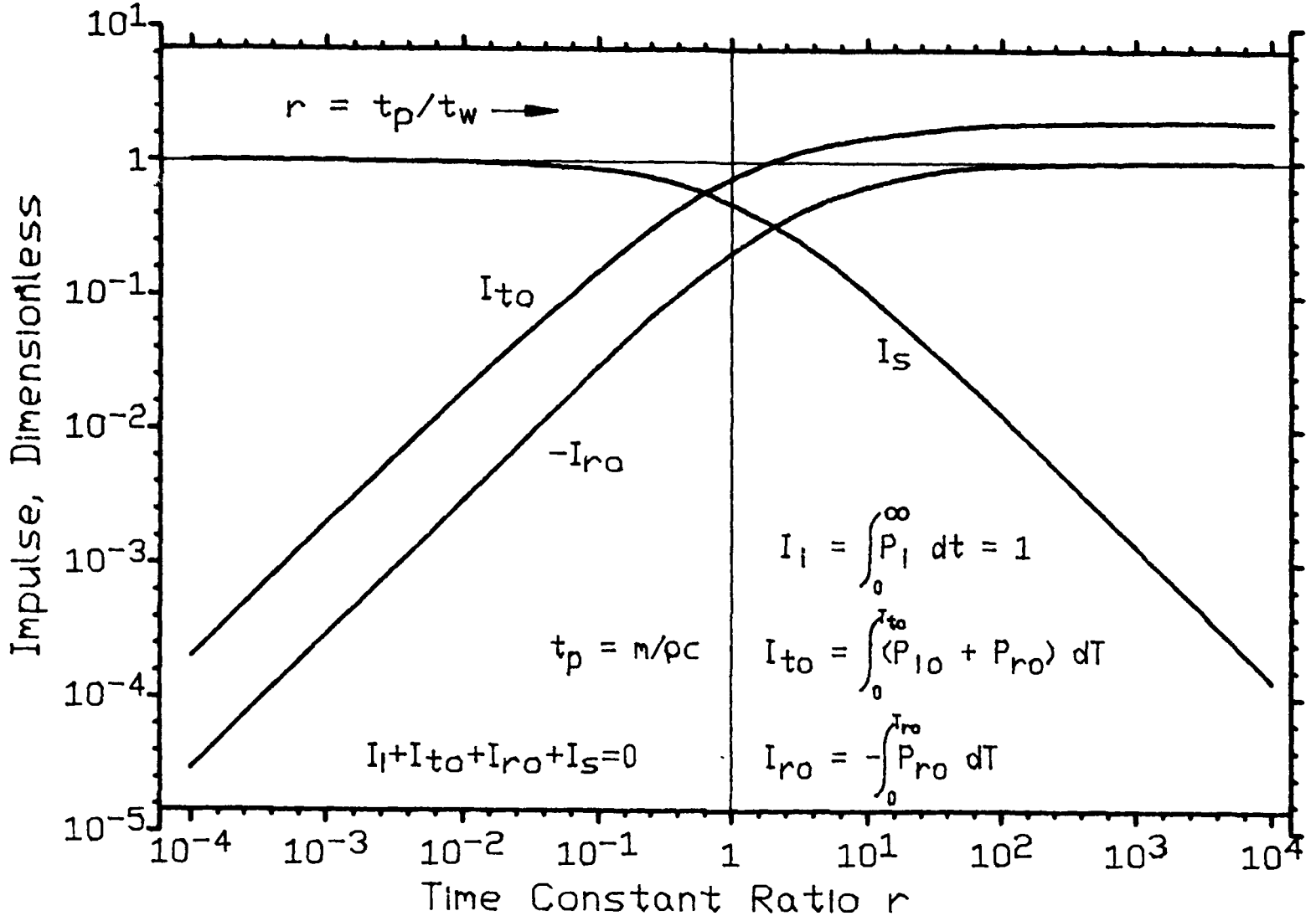

Figure 27. Impulses as a function of time constant ratio r (= t_p/t_w) — for shocked plate.

similar to the well known results for acoustic reflection from a rigid wall: (1) the reflected wave has an impulse equal in magnitude, opposite in direction, to the incident impulse; and (2) the wall receives an impulse equal to twice the incident impulse.

6.4.1 QUALITATIVE DESCRIPTION OF PLATE MOTION.

Figure 28a shows a shock wave impinging perpendicular to hull plating supported by stringers. As an approximation we consider the configuration of figure 28b. Instead of a diaphragm with bending wave, we connect the light weight hull plating by means of a spring to the heavy, rigid hull frame. We look at the beginning motion, while the effect of the spring is small.

Figure 28b implies that the fraction f of the water/hull interface surface has surface load m; fraction (1-f) has surface load M. The simplification we employ is that the total acoustic pressure p_t is at each time the same in (1) the area fraction f, and (2) the area fraction (1-f). In other words we assume that it takes negligible time for pressures to diffract between the area fraction f and the area fraction (1-f).

An example that was considered consists of a 40,000 pound charge of HBX-1 at a distance of 600 to 800 feet from a ship with 1/2 inch plating and drawing 20 feet of water. Then we have

p_o	500	psi
t_w	2.9	msec
ρD	1,280	lbs/ft^2
f	0.8	
m	20.8	lbs/ft^2 .

The overall ship mass is ρD where ρ is the density of seawater and D is the ship draft. The loadings of the partial areas f and (1-f) must collectively support this mass:

$$f.m + (1-f).M = \rho D \quad , \tag{16}$$

so that

$$M = (\rho D - f.m)/(1-f) \quad . \tag{17}$$

Since the hull plate mass m is generally very small compared with the ship mass, we have to a good approximation

$$M = \rho D/(1-f) \quad . \tag{18}$$

If the unsupported portion of the hull plating effectively makes up 80 percent of the hull area, then the massive loading M is 5 times the ship mass per unit area ρD:

M	6,400	lbs/ft^2 .

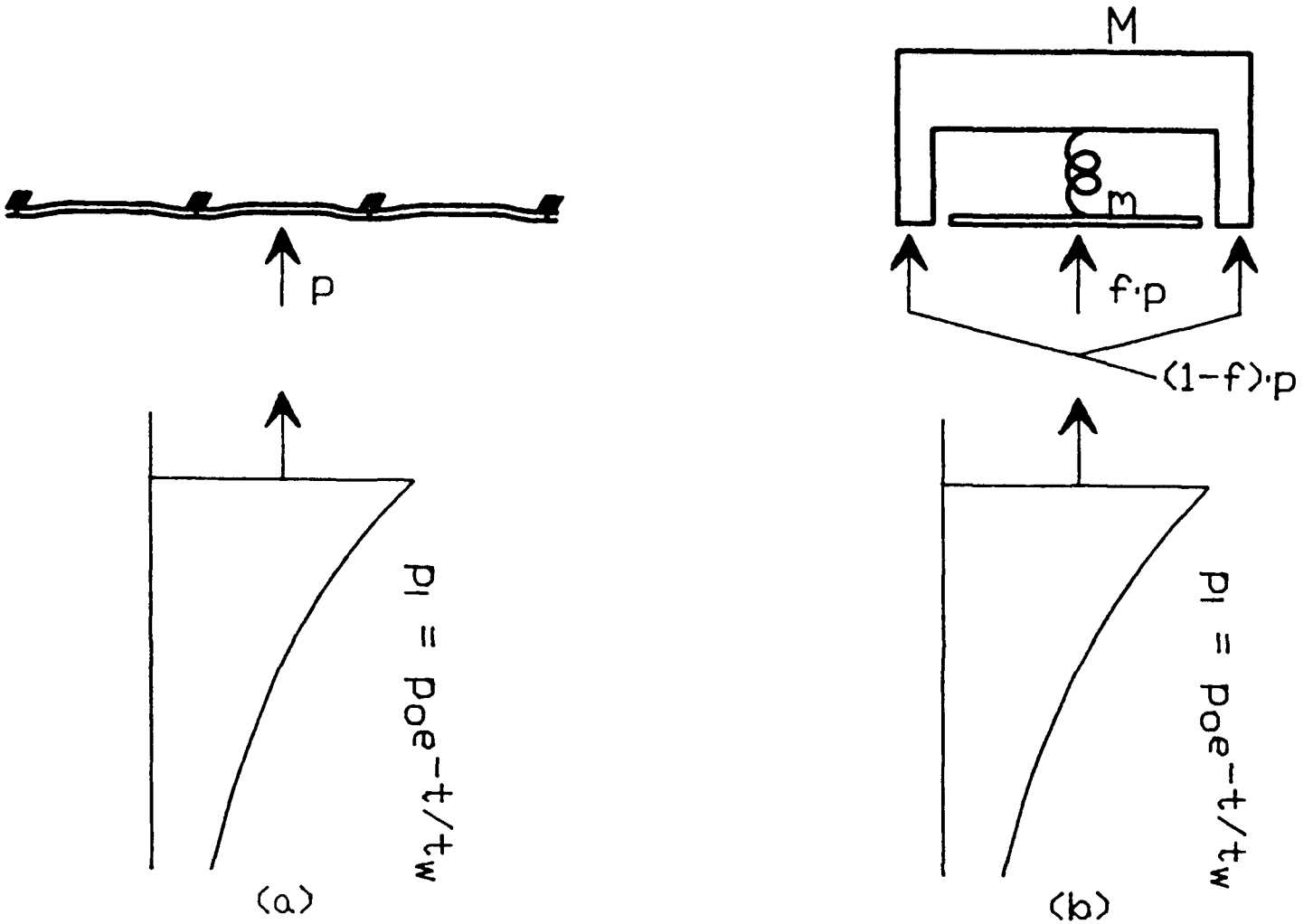

Figure 28. (a) Shock impinging on supported hull plate. (b) Analytical approximation of hull plate.

The damping time constants for m and M are

t_{pm} 2.08 msec
t_{pM} 640 msec ,

and the dimensionless ratios r are

r_m 0.72
r_M 220 .

With these values we see from the graphs of figures 25 through 27 that the stiff hull portions are initially absorbing all the initial impulse; the reflected wave is high pressure. The compliant plate portion rapidly begins to radiate a low pressure wave and traps much of its energy in the kinetic energy of spalled or cavitated water.

As seen in figure 29, the high pressure reflected wave pumps its energy into the low pressure region, exacerbating the trapped kinetic energy there. At some late time this kinetic energy must be absorbed by the hull plate.

Descriptions of major effects have been provided here to the extent feasible without explicitly including diffraction time considerations in the analysis. Rigorous answers require machine numerical solution.

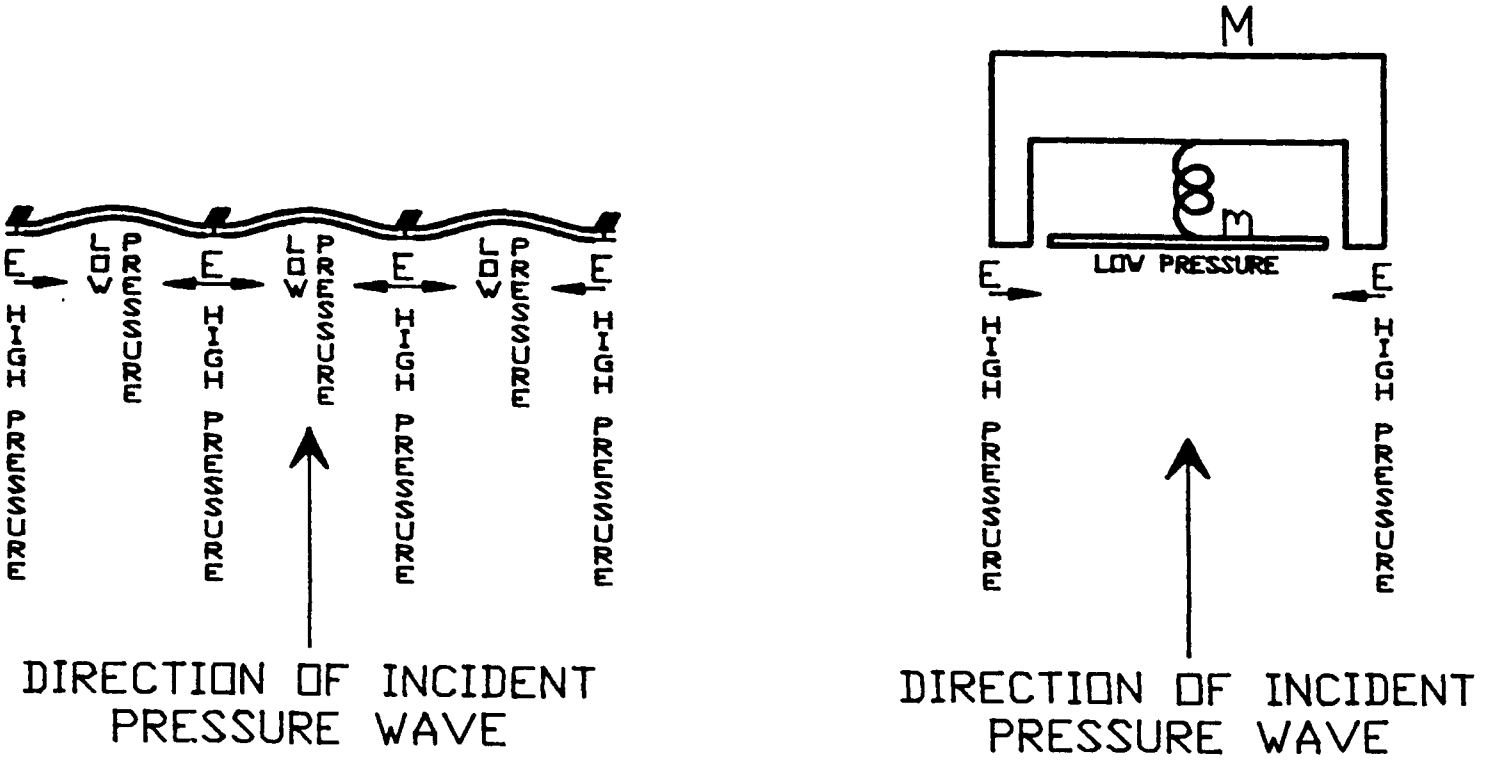

Figure 29. Beginning motion of supported hull plate, showing pumping of high pressure into cavitated region.

SECTION 7

LIST OF REFERENCES

1. Anon, "The Underwater Shock Analysis (USA) Code, A Reference Manual," Lockheed Palo Alto Research Laboratory Final Report DNA 4524F to Defense Nuclear Agency, 28 Feb. 1978.

2. Arons, A. B. and D. R. Yennie, JASA, 22, 1950.

3. Friedlander, F. G, SOUND PULSES, Cambridge University Press, New York 1958.

4. Bedrosian, B, and F. L. DiMaggio, "Acoustic Approximations in Fluid-Shell Interactions," J. Engr. Mech. Div. ASCE, 731, June, 1972.

5. Bleich, H. H, and I. S. Sandler, "Interaction between Structures and Bilinear Fluids," Int. J. Solids and Structures, 66, 617, 1970.

6. Chertock, G, "Transient Flexural Vibrations of Ship-Like Structures Exposed to Underwater Explosions," JASA, 48 (1) (Part 2), 170, 1970.

7. Clarke, Joseph A, "Holographic Visualization Of Acoustic Fields," J. Sound & Vib, 56(2), 167, 1978.

8. ---, "Visual Characteristics of Inhomogeneous Acoustic Waves," J. Sound & Vib, 70(2),267,1980.

9. ---, "Numerical Prediction of Supersonic Bulk-Cavitation Closure Pulses," Catholic University of America Technical Report to Office of Naval Research under Contract No. N00014-76-C-1020, January, 1981.

10. Cole, Robert H, UNDERWATER EXPLOSIONS, Princeton University Press, Princeton, N.J. (1948).

11. Costanzo, Frederick A, and John D. Gordon, "An Analysis of Bulk Cavitation in Deep Water," Underwater Explosive Research Division of the Naval Ship Research and Development Center, Portsmouth, Va. May, 1980.

12. Cushing, Vincent J, and William Losaw, "Hull Plate Deformation from Underwater Shock Waves," Engineering-Physics Co, Final Report to Underwater Explosive Research Division of David Taylor Model Basin under Contract No. N189(181)-56855A(X) (July, 1965).

13. ---, "Study of Bulk Cavitation and Consequent Water Hammer," Engineering-Physics Co. Final Report to ONR under contract Nonr-3389(00), 1961.

14. ---, George Bowden & Dean Reily, "Three-Dimensional Analysis of Bulk Cavitation," Engineering-Physics Co. Interim Report to ONR under contract NONR-3709(00), September 24, 1962.

15. ---, "On The Theory Of Bulk Cavitation," Engineering-Physics Co. Final Report to ONR under Contract No. Nonr-3709(00), December, 1969.

16. ibid, Ch. V, p43 et seq.

17. DeRuntz, J. A, T. L. Geers and C. A. Felippa, "The Underwater Shock Analysis Code, A Reference Manual," Lockheed Palo Alto Research Laboratory, Final Report to Defense Nuclear Agency under contract DNA-001-76-c-0285, February, 1978.

18. DiMaggio, F. L, I. S. Sandler and D. Rubin, "Uncoupling Approximation in Fluid-Structure Interaction Problems with Cavitation," Weidlinger Associates Interim Report to Defense Nuclear Agency under Contracts Nos. DNA 001-79-C-0078 and DNA 001-79-C-0256, February, 1980.

19. F. G. Friedlander, SOUND PULSES, Cambridge University Press, 1958.

20. Gaspin, J. B, and R. S. Price, "The Underpressure Field from Explosions in Water as Modified by Cavitation," NOLTR 72-103, 9 May 1972.

21. Geers, T. L, "Residual Potential and Approximate Methods for Three-Dimensional Fluid-Structure Interaction Problems," JASA, 49(5) (Part 2), 1505 (1971).

22. Haywood, J. H, "Response of and Elastic Cylindrical Shell to a Pressure Pulse," J. Mech. Appl. Math. XI (Part 2), 129 (1958).

23. Huang, H, G. C. Everstine and Y. F. Wang, "Retarded Potential Techniques for the Analysis of Submerged Structures Impinged by Weak Shock Waves," Computational Methods for Fluid-Structures Interaction Problems, ASME 26 (1977).

24. Hudson, G.E, and C.T. Taylor, "Time-Displacement Studies of Diaphragms Deformed by Explosive Loading," Underwater Explosion Research, Vol III, pp. 445-459, ONR, 1950.

25. Kennard, E. H, "Explosive Load on Underwater Structures as Modified by Bulk Cavitation," David Taylor Model Basin Report No. 511, 1943.

26. ---, "Cavitation in an Elastic Liquid," Phys. Rev. 63, 172, 1943.

27. ---, "The Effect of a Pressure Wave on a Plate or Diaphragm," Underwater Explosion Research, Vol III, pp. 9-106, ONR, 1950.

28. Kriebel, A. R, and J. S. Bechtel, "Hydrodynamic Data from Exploding Wires," URS Research Co Annual Report URS 679-6 to ONR under contract N0014-67-C-0451, April 1, 1970.

29. Mindlin, R. D, and H. H. Bleich, "Response of an Elastic Cylindrical Shell to a Transverse, Step Shock Wave," J. Appl. Mech. 20, 189, 1953.

30. Mnev, Y. N, and A. K. Pertsev, "Hydroelasticity of Shells," Translation Division, Foreign Technical Division, Wright-Patterson AFB, FTD-MT-24-119-71.

31. Murray, W. W, "Model Studies of Underwater Atomic Explosions on Ships, Part V, Results of Panel Tests," UERD Rept 3-58, 1948.

32. NAVSEA 0908-LP-000-0010, "Test Plan For Routine Shock Testing of Ships," Naval Ship Engineering Center, Hyattsville, Maryland, January, 1975.

33. Newton, R. E, "Effects of Cavitation on Underwater Shock Loading," Naval Postgraduate School Interim Report NPS-69-78-013 to Defense Nuclear Agency under MIPR 78-654, July, 1978.

34. ---, "Effects of Cavitation in Underwater Shock Loading," Naval Postgraduate School Final Report to Defense Nuclear Agency under Grant No. MIPR 79-608, April, 1980.

35. Officer, C. B, **SOUND TRANSMISSION**, McGraw-Hill, New york City, 1958.

36. Ranlet, D, F. L. DiMaggio, H. H. Bleich and M. L. Barron, "Elastic Response of Submerged Shells with Internally Attached Structures to Shock Loading," **Computers and Structures**, 7, 355, 1977.

37. Rehak, Margareta L, Frank L. DiMaggio and Ivan S. Sandler, "Interactive Approximations for a Cavitating Fluid around a Floating Structure," **Computers and Structures**, 21, NO.6, 1159, 1985.

38. ---, M, R. Smilowitz and R. Kagel, "The FRAM Cavitation Code," Weidlinger Associates Technical Report DNA-TR-86-179 to Defense Nuclear Agency under contract DNA-001-84-C-0001, 15 May 1986.

39. Reily, Dean, "Hydro Shock Experiment," Engineering-Physics Co. Final Report, ONR Contract No. N000 14-69-C-1238, 7 Jan. 1970.

40. Sachs, David A, "Underwater Shockwave Focusing at Caustics," Cambridge Acoustical Associates Final Report U-322-188 to ONR under contract N00014-66-C-0110, 31 Aug. 1969.

41. Schauer, Heinrich N, UERD Rept. 17-49, Nov, 1949.

42. ---, UERD Rept. 4-50, May, 1950.

43. Schultz, Michael E, and Vincent J. Cushing, "Surface Velocity Measurements at Mono Lake," Engineering-Physics Co. to ONR under contract No. N00014-66-C-0165 for Office of Naval Research, Washington, D.C, August, 1970.

44. Smilowitz, R, R. Kagel and I. Sandler, "Shock Response of a Partially Submerged Linearly Elastic Structure (User's Manual for the SRUE Code)," Weidlinger Associates Technical Report DNA-TR-86-25 to Defense Nuclear Agency under contract DNA-001-84-C-0001, 10 Jan. 1986.

45. Taylor, G. I, "The Pressure and Impulse of Submarine Explosion Waves on Plates," Underwater Explosion Research, Vol. I, pp. 115-1173, ONR, 1950.

46. Waldo, G. V, "A Bulk Cavitation Theory with a Simple Exact Solution," NSRDC, Washington, DC, Rpt 3010, April, 1969.

47. Walker, R. R, and J. D. Gordon, "A study of the Bulk Cavitation Caused by Underwater Explosions," DTMB Report 1896, 1966.

48. Wentzell, R. A, "Cavitation Due to Shock Pulses Reflected from the Sea Surface," JASA, 46, No.3 (part 2), 1969.

APPENDIX

BULK CAVITATION
Z100 Basic Program

```
10 ' CAVIT.7CN    BASIC VERSION
12 GOTO 40
20 CLS: LOCATE 4,1
22 PRINT "           ********** FORTRAN VERSION OF 'CAVIT' ********"
24 PRINT "           ***ORIGINAL PROGRAM BY COSTANZO AND GORDON****"
26 PRINT "           ****   UERD/DINSRDC     (DNA).              *****"
28 PRINT "           ****   9 OCT, 1980 REVISION TO INCLUDE     *****"
30 PRINT "           **** EFFECTS OF BOTTOM LAYER ACCELERATION*****"
32 PRINT "           ****   BY J. CLARK      (CUA).              *****"
34 PRINT "           ****   23 DEC 1987 REVISION TO INCLUDE     *****"
35 PRINT "           ****  UPPER BOUNDARY DYNAMICS, AFTERFLOW  *****"
36 PRINT "           ****  AND CLOSURE MACH NUMBER             *****"
37 PRINT "           ****   BY V. CUSHING    (CAI).              *****"
38 PRINT "           ************************************************"
39 RETURN
40 WIDTH LPRINT 100
50 FF$ = CHR$(12): QUOTE$ = CHR$(34): CR$ = CHR$(13)
60 DEF FNNU$(I,J) = RIGHT$(SPACE$(J-1)+STR$(I),J)
70 DEF FNN$(I) = MID$(STR$(I),2)
80 '' KEY 7,"SAVE"+QUOTE$+"L.L"+QUOTE$+",A"+CR$
90 '' KEY 9, "SYSTEM"+CR$
100 '' KEY 8, "LPRINT FF$" + CR$
110 DEFINT I-N: DEFSTR S
120 : DIM R(200), Z(200,3), T(200,3), ZSDOT(200), ZBDOT(200), DELDOT(200),
        RMACH(200)
122 N1 = 5: N2 = 4: SFORM2 = STRING$(N1,"#") + "." + STRING$(N2,"#"): NN =
        N1+N2+1: SFORM1 = "\" + SPACE$(NN-2) + "\"
500 ' INITIALIZATION
510 PATMOS = 14.7*144: RHO = 2: GEE = 32.2: CWAT = 5000
520 GAMMA = RHO*GEE: AINT = 2*RHO/PATMOS ' <---> PSI IN INTEGRAL (TOTAL IN
        LINE)
530 RSTART = 200
540 AIMP = RHO*CWAT
550  AK  =  144*23976:  AL  =  1.13:  AM  =  .0654*.001:  AN  =  -.18  '  HBX-1
PARAMETERS
554 GOSUB 20
555   INPUT "                                    OUTPUT FILE NAME : ", SOUT
556   INPUT "                                        POUNDS OF HE : ", W
570 W3 = W^.333
574   INPUT "                                         BURST DEPTH : ", D
580   PRINT "           PROGRAM IS NOW COMPUTING MAXIMUM CAVITY RADIUS"
590 NDZ = 500
1000 ' ENTRY POINT
1010 GOSUB 8000
1020  PRINT "                          THE MAXIMUM CAVITY RADIUS IS : " R(0)
1022  INPUT "          # RADIAL DATA POINTS AS N#; OR DR AS D#: ", S
1024 IF LEFT$(S,1) = "N" THEN DELRAD = R(0)/VAL(MID$(S,2))
1026 IF LEFT$(S,1) = "D" THEN DELRAD = VAL(MID$(S,2))
1030  PRINT "                PROGRAM IS NOW COMPUTING VERTICAL BOUNDS": LIN =
        CSRLIN: GOSUB 9000
1040  PRINT "                       PROGRAM IS NOW COMPUTING CLOSURE": LIN =
        LIN+1: GOSUB 10000
1044  PRINT "                        PROGRAM IS NOW WRITING TO FILE":
        GOSUB 15000
1050 ' PLOT CLOSURE WAVE
1054 PRINT SPACE$(N1-2);
1060 PRINT USING SFORM1; "  R  "; "Z-UPPER"; "Z-LOWER"; "Z-CLOSE";
        "T-CLOSE"; "ZSDOT"; "ZBDOT"; "1/MACH"
1070 FOR I = 1 TO IMAX
1080 PRINT USING SFORM2; R(I); Z(I,1); Z(I,2); Z(I,3); T(I,3); ZS DOT(I);
        ZBDOT(I); RMACH(I)
1082 NEXT I
1100 SYSTEM
1200 END
2000 '--------------- SUBROUTINE LOWER(R,Z)
2010 Z = 0: GOSUB 7000: FMEM = F: XMEM = Z
2020 Z = 2.5: IFLAG = 0: ICOUNT = 0
```

```
2030 GOSUB 7000: X = Z
2040 GOSUB 4000: Z = X
2050 IF IFLAG = 0 GOTO 2030
2070 RETURN
2080 '
3000 '--------------- SUBROUTINE UPPER(R,Z)
3010 Z = 0: GOSUB 5000: FMEM = F: XMEM = Z ' 5000 REQUIRES R,Z
3020 Z = .1: IFLAG = 0: ICOUNT = 0
3030 GOSUB 5000: X = Z
3040 GOSUB 4000 : Z = X
3050 IF IFLAG = 0 GOTO 3030
3060 GOSUB 6500: T = TAR
3070 RETURN
3080 '
4000 '--------------- SUBROUTINE FOR F ---> 0
4010 XNEW = X - F*(X-XMEM)/(F-FMEM)
4020 XDIF = ABS(XNEW-X)
4030 XMIN = .05
4040 IF (XDIF < XMIN) THEN IFLAG = 1
4050 XMEM = X
4060 X = XNEW
4070 FMEM = F
4090 RETURN
4100 '
5000 '--------------- SUBROUTINE UPP1(R,Z,F)
5010 GOSUB 6000
5020 F = -PREL - AK*((W3/RA)^AL)
5030 RETURN
5040 '
6000 '--------------- SUBROUTINE PRESS(R,Z,PREL)
6010 GOSUB 6500
6020 THETAI = AM*W3*((W3/RI)^AN)
6030 PI0 = AK*((W3/RI)^AL)
6040 PINC = PI0*EXP(-TI/THETAI)
6042 UI = (PI0/AIMP)*( THETAI/TI0 + ( 1-THETAI/TI0)*( EXP(-TI/THETAI) ) )
       ' INCLUDING AFTERFLOW
6050 PHYD = GAMMA*Z
6060 PREL = -(PINC + PATMOS + PHYD): UA = PREL/AIMP
6090 UZ = -UI*(D-Z)/RI + UA*(D+Z)/RA: UR = UI*R/RI + UA*R/RA
6100 RETURN
6500 '_____________ T SUBROUTINE
6510 RI = SQR(R*R + (D-Z)^2): RA = SQR(R*R + (D+Z)^2)
6520 TAR = RA/CWAT: TI0 = RI/CWAT: TI = TAR - TI0
6530 RETURN
6540 '
7000 '--------------- SUBROUTINE  LOW1(R,ZB,G3)
7010 GOSUB 6000
7020 F1 = (D + Z)/RA
7030 FI2 = (RA - 2*D*F1)/RI
7040 F = -(1 + FI2*(AN*RA/RI - AN -1))*PINC/(CWAT*THETAI)
7050 F = F - AL*FI2*PINC/RI
7060 F = F + GAMMA*F1 - AL*PREL/RA
7070 RETURN
7080 '
8000 '--------------- SUBROUTINE TANPT(R3)
8010 R = RSTART
8030 GOSUB 3000: GOSUB 7000: RMEM = R: GMEM = F
8040 R = 2*R
8060 GOSUB 3000: GOSUB 7000: IFLAG = 0
8070 X = R: XMEM = RMEM: FMEM = GMEM: GOSUB 4000: R = X: RMEM = XMEM:
       GMEM = FMEM
8080 IF IFLAG = 0 GOTO 8060
8100 R(0) = R
8110 RETURN
8120 '
9000 '--------------- SUBROUTINE BOUNDS(R(0))
9010 R = 0: I = 1: FINAL = R(0) + .5*DELRAD
9020 LOCATE 16,1: PRINT "RADIAL COMPUTATION #: ": GOSUB 20000
       ' PRINT COUNTER
9030 GOSUB 3000
9040 Z(I,1) = Z: T(I,1) = TAR
9050 GOSUB 2000
```

```
9060 Z(I,2) = Z: T(I,2) = TAR: R(I) = R
9070 IF Z > Z2MAX THEN Z2MAX = Z
9090 R = R + DELRAD: I = I + 1
9100 IF R < FINAL GOTO 9020
9110 IMAX = I-1
9120 RETURN
9130 '
10000 '--------------- SUBROUTINE CCURVE
10010 FOR I = 1 TO IMAX
10020 DZ = Z2MAX/NDZ
10030 R = R(I)
10040 GOSUB 20000
10060 '
10100 ' ----------------- SET UP BOTTOM FACTORS
10110 Z = Z(I,2)
10120 GOSUB 6000
10130 TA = TAR: TE = TI: TI1 = TI0
10140 THETA = THETAI
10150 COEF1 = -PI0/AIMP: CONST1 = THETA/TI1: COEF2 = 1 - CONST1
10160 COEF3 = COEF1*THETA: COEF4 = CONST1 - 1: CONST2 = EXP(-TE/THETA)
10170 FACTVI = (D-Z)/RI: FACTVA = (D+Z)/RA
10180 FACTRI = R/RI: FACTRA = R/RA
10190 UA0 = UA
10210 Z = 0: GOSUB 6000: UZMEM = UZ
10220 TOTAL = 0: ZMEM = 0: ZB = 0: ZS = 0: ZSMEM = 0: TTMEM = TAR:
      IFLAG2 = 0
10230 GOSUB 10500: FMEM = F
10240 Z = DZ: ICOUNT = 0
10250 '
10300 ' ------------------- CLOSURE COMPUTATION
10310 GOSUB 11000
10320 IF IFLAG2 = 1 GOTO 10360
10330 IF ZB < ZS THEN IFLAG = 0: IFLAG2 = 1: GOSUB 10500: FMEM = F:
      XMEM = Z: Z = Z - DZ: GOTO 10310 ' CHANGE TO F ROUTINE
      FOR CONVERGENCE
10340 Z = Z + DZ
10350 GOTO 10300
10360 GOSUB 10500
10370 X = Z: GOSUB 4000: Z = X
10380 IF IFLAG = 0 THEN ZMEM = XMEM: GOTO 10300
10390 GOSUB 11000
10400 IF I = 1 THEN RMACH(I) = 0: GOTO 10420
10410 DS = SQR( (R-RLAST)^2 + (Z-ZLAST)^2 ): DT = TT - TLAST: RMACH(I) =
      DT*CWAT/DS
10420 RLAST = R: TLAST = TT: ZLAST = Z
10430 Z(I,3) = Z: T(I,3) = TT: ZSDOT(I) = ZSDOT: ZBDOT(I) = ZBDOT:
      DELDOT(I) = ZSDOT - ZBDOT
10480 NEXT I
10490 RETURN
10500 ' ------------- SET UP F FOR CLOSURE
10510 F = ZS - ZB
10520 RETURN
10530 '
11000 ' ----------------- START LOOP WITH SURFACE MOTION
11010 GOSUB 6000
11020 IF IFLAG2 = 1 THEN DZ = Z - ZMEM
11030 TOTAL = TOTAL + .5*(UZ + UZMEM)*DZ: UZMEM = UZ
11040 TF = AINT*(Z*UZ - TOTAL) ' TIME OF FLIGHT TF (SEC) AS FUNCTION OF
      SPALL THICKNESS Z (FEET)
11050 ZR = UR*TF
11060 ZS = TF*UZ + .5*GEE*TF*TF ' SURFACE DISPLACEMENT --- EQS. 14 AND
            18 REFERENCE 15
11070 TT = TAR + TF ' TT = TOTAL OR ACTUAL TIME
11080 DELT = TT-TTMEM
11084 IF ABS(DELT) < .000003 GOTO 11100
11090 ZSDOT = (ZS-ZSMEM)/DELT
11100 ZSMEM = ZS: ZMEM = Z: TTMEM = TT
11110 IF TT < TA THEN Z = Z + DZ: GOTO 11000
11200 ' ----------------- BEGIN BOTTOM MOTION CALCULATION
11210 T = TT-TI1
11220 VI = COEF1*( COEF2*EXP(-T/THETA) + CONST1 )
11230 ZI = COEF3*(  ( EXP(-T/THETA) - CONST2 )*COEF4 + (T-TE)/TI1  )
```

```
        ' REFERENCE 11, EQ. 23 -- NEGATIVE (UPWARD) DISPLACEMENT
11240 T = TT-TA
11250 VA = UA0*(1 + T/TA)
11260 ZA = UA0*T*(1 + .5*T/TA) ' EQ. 24
11270 ZBR = ZI*FACTRI + ZA*FACTRA: ZBRDOT = VI*FACTRI + VA*FACTRA
11280 ZB = ZI*FACTVI + ZA*FACTVA: ZBDOT = VI*FACTVI + VA*FACTVA
11300 RETURN
11310 '
15000 '--------------- SUBROUTINE DFILE
15010 OPEN "O", #1, SOUT
15011 PRINT #1, SPACE$(N1-2);
15012 PRINT #1, USING SFORM1; "  R  "; "Z-UPPER"; "Z-LOWER"; "Z-CLOSE"; "T-
      CLOSE"; "ZSDOT"; "ZBDOT"; "1/MACH"
15020 FOR I = 1 TO IMAX
15030 PRINT #1, USING SFORM2; R(I); Z(I,1); Z(I,2); Z(I,3); T(I,3); (I);
      ZSDOT(I); ZBDOT(I); RMACH(I)
15044 NEXT I
15046 CLOSE #1
15050 RETURN
```

DISTRIBUTION LIST

DNA-TR-89-289

DEPARTMENT OF DEFENSE

ASSISTANT TO THE SECRETARY OF DEFENSE
ATTN: EXECUTIVE ASSISTANT

DEFENSE INTELLIGENCE AGENCY
ATTN: DB-4C3
ATTN: DB-6E1
ATTN: DB-6E2 C WIEHLE
ATTN: RTS-2B

DEFENSE NUCLEAR AGENCY
ATTN: OPNS
ATTN: SPSD
ATTN: SPSD LCDR C NOFZIGER
ATTN: SPWE
ATTN: SPWE A FREDERICKSON
ATTN: SPWE E TREMBA
ATTN: SPWE LCDR M O'BRYANT
4 CYS ATTN: TITL

DEFENSE NUCLEAR AGENCY
ATTN: TDNV

DEFENSE NUCLEAR AGENCY
ATTN: TDNM
ATTN: TDTT

DEFENSE TECHNICAL INFORMATION CENTER
2 CYS ATTN: DTIC/FDAB

FIELD COMMAND DEFENSE NUCLEAR AGENCY
ATTN: FCPR

THE JOINT STAFF
ATTN: JKC (ATTN: DNA REP)
ATTN: JKCS

DEPARTMENT OF THE ARMY

DEP CH OF STAFF FOR OPS & PLANS
ATTN: DAMO-SWN

ENGINEER STUDIES CENTER
ATTN: SECURITY MANAGER

HARRY DIAMOND LABORATORIES
ATTN: SLCIS-IM-TL

U S ARMY CORPS OF ENGINEERS
ATTN: CERD-L

U S ARMY ENGR WATERWAYS EXPER STATION
ATTN: C WELCH CEWES-SE-R
ATTN: CEWES J K INGRAM
ATTN: CEWES-CW D OUTLAW
ATTN: CEWES-SD J G JACKSON, JR
ATTN: J ZELASKO CEWES-SD-R
ATTN: R WHALIN CEWES-ZT
ATTN: RESEARCH LIBRARY
ATTN: S HUGHES

U S ARMY FOREIGN SCIENCE & TECH CTR
ATTN: AIFRTA

U S ARMY MATERIAL TECHNOLOGY LABORATORY
ATTN: DRXMR J MESCALL
ATTN: TECHNICAL LIBRARY

U S ARMY MISSILE COMMAND/AMSMI-RD-CS-R
ATTN: AMSMI-RD-CS-R

U S ARMY NUCLEAR & CHEMICAL AGENCY
ATTN: MONA-NU D BASH

U S ARMY STRATEGIC DEFENSE COMMAND
ATTN: CSSD-SA-EV
ATTN: CSSD-SL

U S ARMY WAR COLLEGE
ATTN: LIBRARY

USA SURVIVABILITY MANAGMENT OFFICE
ATTN: SLCSM-SE J BRAND

DEPARTMENT OF THE NAVY

DAVID TAYLOR RESEARCH CENTER
ATTN: CODE 11
ATTN: CODE 172
ATTN: CODE 173
ATTN: CODE 1740.1
ATTN: CODE 1740.4
ATTN: CODE 1740.5
ATTN: CODE 1740.6
ATTN: CODE 1770.1
ATTN: CODE 2740

MAGTF WARFIGHTING CENTER
ATTN: D091 J HARTNEADY

MARINE CORPS
ATTN: CODE POR-21

NAVAL COASTAL SYSTEMS CENTER
ATTN: CODE 7410

NAVAL DAMAGE CONTROL TRAINING CENTER
ATTN: COMMANDING OFFICER

NAVAL ELECTRONICS ENGRG ACTVY, PACIFIC
ATTN: CODE 250

NAVAL EXPLOSIVE ORD DISPOSAL TECHNOLOGY CENTER
ATTN: CODE 90 J PETROUSKY

NAVAL POSTGRADUATE SCHOOL
ATTN: B K WOEHLER
ATTN: CODE 1424 LIBRARY

NAVAL RESEARCH LABORATORY
ATTN: CODE 2627
ATTN: CODE 5100
ATTN: CODE 6380

NAVAL SEA SYSTEMS COMMAND
ATTN: PMS 421B A COTE, JR
ATTN: SEA-033
ATTN: SEA-08
ATTN: SEA-09G53
ATTN: SEA-323
ATTN: SEA-55X
ATTN: SEA-55X1
ATTN: SEA-55Y
ATTN: SEA-9931G

NAVAL SURFACE WARFARE CENTER
ATTN: CODE H21
ATTN: CODE R14
ATTN: CODE R15
ATTN: CODE U401 M KLEINERMAN

NAVAL SURFACE WARFARE CENTER
ATTN: CODE K42 R ROBINSON
ATTN: TECHNICAL LIBRARY

NAVAL WEAPONS CENTER
ATTN: CODE 3263 J BOWEN

NAVAL WEAPONS EVALUATION FACILITY
ATTN: CLASSIFIED LIBRARY

NEW LONDON LABORATORY
ATTN: CODE 4492 J KALINOWSKI
ATTN: CODE 4494 J PATEL
ATTN: TECH LIBRARY

OFFICE OF CHIEF OF NAVAL OPERATIONS
ATTN: NOP 098T8
ATTN: NOP 223
ATTN: NOP 225
ATTN: NOP 37
ATTN: NOP 605D5
ATTN: NOP 957E
ATTN: OP 03EG
ATTN: OP 21
ATTN: OP 654
ATTN: OP 73
ATTN: OP 02

OFFICE OF NAVAL RESEARCH
ATTN: CODE 1132SM

THEATER NUCLEAR WARFARE PROGRAM OFC
ATTN: PMS-42332C

US NAVAL ACADEMY
ATTN: LIBRARY

DEPARTMENT OF THE AIR FORCE

AIR FORCE INSTITUTE OF TECHNOLOGY/EN
ATTN: COMMANDER

HEADQUARTERS USAF/IN
ATTN: IN

HQ USAF/CCN
ATTN: AFCCN

ROME AIR DEVELOPMENT CENTER, AFSC
ATTN: COMMANDER

USAF/LEEEU
ATTN: LEEE

WEAPONS LABORATORY
ATTN: NTE
ATTN: NTED G GOODFELLOW
ATTN: NTED R HENNY
ATTN: NTES
ATTN: WL/SUL

DEPARTMENT OF ENERGY

DEPARTMENT OF ENERGY
OFFICE OF MILITARY APPLICATIONS
ATTN: OMA/DP-225

LAWRENCE LIVERMORE NATIONAL LAB
ATTN: C E ROSENKILDE
ATTN: D MAGNOLI

LOS ALAMOS NATIONAL LABORATORY
ATTN: T DOWLER
ATTN: REPORT LIBRARY

MARTIN MARIETTA ENERGY SYSTEMS INC
ATTN: CIVIL DEF RES PROJ
ATTN: CENTRL RESRCH LIB 4500N

SANDIA NATIONAL LABORATORIES
ATTN: DIV 9311 J S PHILLIPS
ATTN: TECH LIB 3141

OTHER GOVERNMENT

CENTRAL INTELLIGENCE AGENCY
ATTN: OSWR/NED

DEPARTMENT OF THE INTERIOR
ATTN: D RODDY

U S NUCLEAR REGULATORY COMMISSION
ATTN: R WHIPP FOR L SHAO

DEPARTMENT OF DEFENSE CONTRACTORS

AMI RESEARCH
ATTN: V GODINO

APPLIED RESEARCH ASSOCIATES, INC
ATTN: R FRANK

BDM INTERNATIONAL INC
ATTN: E DORCHAK

BOEING TECHNICAL & MANAGEMENT SVCS, INC
ATTN: R SCHMIDT

CALIFORNIA INSTITUTE OF TECHNOLOGY
ATTN: T AHRENS

CALIFORNIA RESEARCH & TECHNOLOGY, INC
ATTN: K KREYENHAGEN
ATTN: LIBRARY
ATTN: M ROSENBLATT
ATTN: S SCHUSTER

CALIFORNIA RESEARCH & TECHNOLOGY, INC
ATTN: J THOMSEN
ATTN: R ENGLAND

CALIFORNIA, UNIVERSITY AT SAN DIEGO (A-030)
ATTN: W VAN DORN

COLUMBIA UNIVERSITY
ATTN: F DIMAGGIO

CUSHING ASSOCIATES, INC
2 CYS ATTN: V J CUSHING

DENVER COLORADO SEMINARY UNIVERSITY OF
ATTN: J WISOTSKI

ENGINEERING METHODS & APPLICATIONS INC
ATTN: DAVID DIVOKY

KAMAN SCIENCES CORP
ATTN: L MENTE
ATTN: LIBRARY
ATTN: R RUETENIK

KAMAN SCIENCES CORP
ATTN: F SHELTON
ATTN: LIBRARY B KINSLOW

KAMAN SCIENCES CORP
ATTN: DASIAC
ATTN: E CONRAD

KAMAN SCIENCES CORPORATION
ATTN: DASIAC

KARAGOZIAN AND CASE
ATTN: J KARAGOZIAN

LOCKHEED MISSILES & SPACE CO, INC
ATTN: PHILIP UNDERWOOD

LOCKHEED MISSILES & SPACE CO, INC
ATTN: TECH INFO CTR

MCDONNELL DOUGLAS CORPORATION
ATTN: R HALPRIN

MIAMI, UNIVERSITY OF
ATTN: B LEMEHAUTE
ATTN: S WANG

NEW MEXICO ENGINEERING RESEARCH INSTITUTE
ATTN: J JARPE
ATTN: N BAUM

PACIFIC-SIERRA RESEARCH CORP
ATTN: H BRODE

PHYSICS APPLICATIONS, INC
ATTN: DOCUMENT CONTROL

R & D ASSOCIATES
ATTN: B LEE

R & D ASSOCIATES
ATTN: E FURBEE
ATTN: J WEBSTER

RAND CORP
ATTN: B BENNETT

ROSENSTIEL SCHOOL OF MARINE
ATTN: APPL MAR PHYSICS-GROSVENOR
ATTN: APPL MAR PHYSICS-MSC124

S-CUBED
ATTN: K D PYATT, JR
ATTN: R SEDGEWICK

SCIENCE APPLICATIONS INTL CORP
ATTN: DR M MCKAY
ATTN: H WILSON
ATTN: TECHNICAL REPORT SYSTEM

SCIENCE APPLICATIONS INTL CORP
ATTN: G BINNINGER

SCIENCE APPLICATIONS INTL CORP
ATTN: R ALLEN

SCIENCE APPLICATIONS INTL CORP
ATTN: J R BRITT

SRI INTERNATIONAL
ATTN: D KEOUGH
ATTN: J COLTON
ATTN: M SANAI
ATTN: P DE CARLI

TELEDYNE BROWN ENGINEERING
ATTN: J RAVENSCRAFT

TRW INC
ATTN: TECH INFO CTR

TRW SPACE & DEFENSE SECTOR SPACE
ATTN: OUT6 W WAMPLER

WEIDLINGER ASSOC, INC
ATTN: J ISENBERG

WEIDLINGER ASSOCIATES, INC
ATTN: T DEEVY

WEIDLINGER ASSOCIATES, INC
ATTN: M BARON

WESTINGHOUSE ELECTRIC CORP
ATTN: D BOLTON